Eur. Phys. J. B **42**, 509–528 (2004)
DOI: 10.1140/epjb/e2005-00010-2

THE EUROPEAN PHYSICAL JOURNAL B

Excitons dressed by a sea of excitons

M. Combescot[a] and O. Betbeder-Matibet

GPS, Université Pierre et Marie Curie, CNRS, Campus Boucicaut, 140 rue de Lourmel, 75015 Paris, France

Received 5 May 2004 / Received in final form 10 November 2004
Published online 18 January 2005 –

Abstract. We here consider an exciton i embedded in a sea of N identical excitons 0. If the excitons are taken as true bosons, a bosonic enhancement factor N is found for $i = 0$. If the exciton composite nature is kept, this enhancement not only exists for $i = 0$, but also for any exciton having a center of mass momentum equal to the sea exciton momentum. This physically comes from the fact that an exciton with such a momentum can be transformed into a sea exciton by "Pauli scattering", i.e., carrier exchange with the sea, making this exciton i not so much different from a sea exciton. This possible scattering, directly linked to the composite nature of the excitons, is irretrievably lost when the excitons are bosonized. The underlying interest of this work is in fact the calculation of the scalar products of N-exciton states, which turns out to be quite tricky, due to possible carrier exchanges between excitons. This work actually constitutes a crucial piece of our many-body theory for interacting composite bosons, because all physical effects involving composite bosons ultimately end by the calculation of such scalar products. The "skeleton diagrams" we here introduce to represent them, allow to visualize many-body effects linked to carrier exchanges in an easy way. They are conceptually different from Feynman diagrams, because of the special feature of the Pauli scatterings which originate from boson statistics departure.

PACS. 71.35.-y Excitons and related phenomena

1 Introduction

We are presently developing a many-body theory [1–7] able to handle interactions between composite bosons, such as the semiconductor excitons. The development of this theory is highly desirable, because, in the low density limit, electron-hole pairs are known to form bound excitons, so that, in this limit, the representation of the system in terms of excitons is surely better than the one in terms of free carriers. The interaction *between* excitons is however a quite tricky concept due to carrier indistinguishability: Indeed, the Coulomb interaction between two excitons can be taken as $(V_{ee'} + V_{hh'} - V_{eh'} - V_{e'h})$ or $(V_{ee'} + V_{hh'} - V_{eh} - V_{e'h'})$ depending if we see the excitons as made of (e, h) and (e', h'), or of (e, h') and (e', h). Moreover, excitons interact in a far more subtle manner through Pauli exclusion between their indistinguishable components, *in the absence of any Coulomb process.* This "Pauli interaction" is actually the novel and interesting part of our new many-body theory for composite bosons. It basically comes from boson statistics departure, all previous many-body theories, designed for true bosons or true fermions, having the corresponding commutation rules set up in the first line, through the Green function T-products [8]. In our theory, the fact that excitons are not exact bosons appears through "Pauli scatterings" λ_{mnij} between the "in" excitons (i, j) and the "out" excitons (m, n). Their link to boson departure is obvious from their definition [2,3],

$$[B_m, B_i^\dagger] = \delta_{mi} - D_{mi}, \tag{1}$$

$$[D_{mi}, B_j^\dagger] = 2 \sum_n \lambda_{mnij}\, B_n^\dagger, \tag{2}$$

$B_i^\dagger$ being the i exciton creation operator. These Pauli scatterings λ_{mnij} precisely read

$$\lambda_{mnij} = \frac{1}{2} \int d\mathbf{r}_e\, d\mathbf{r}_{e'}\, d\mathbf{r}_h\, d\mathbf{r}_{h'}\, \phi_m^*(\mathbf{r}_e, \mathbf{r}_h) \phi_n^*(\mathbf{r}_{e'}, \mathbf{r}_{h'}) \times \phi_i(\mathbf{r}_e, \mathbf{r}_{h'})\, \phi_j(\mathbf{r}_{e'}, \mathbf{r}_h) \;+\; (m \leftrightarrow n), \tag{3}$$

where $\phi_i(\mathbf{r}_e, \mathbf{r}_h) = \langle \mathbf{r}_e, \mathbf{r}_h | B_i^\dagger | v \rangle$ is the i exciton wave function. The above expression makes clear that λ_{mnij} just corresponds to the two possible carrier exchanges between the two excitons (i, j), (see Fig. 1a), without any Coulomb process: This makes λ_{mnij} a dimensionless "scattering". It is possible to show that, for bound states, λ_{mnij} is of the order of $\mathcal{V}_X/\mathcal{V}$, with $\mathcal{V}_X$ being the exciton volume and $\mathcal{V}$ the sample volume [6].

Although not always straightforward, it is in fact possible to write any physical quantity dealing with excitons, through matrix elements of an Hamiltonian dependent operator $f(H)$ between N-exciton states, with most of them

[a] e-mail: combescot@gps.jussieu.fr

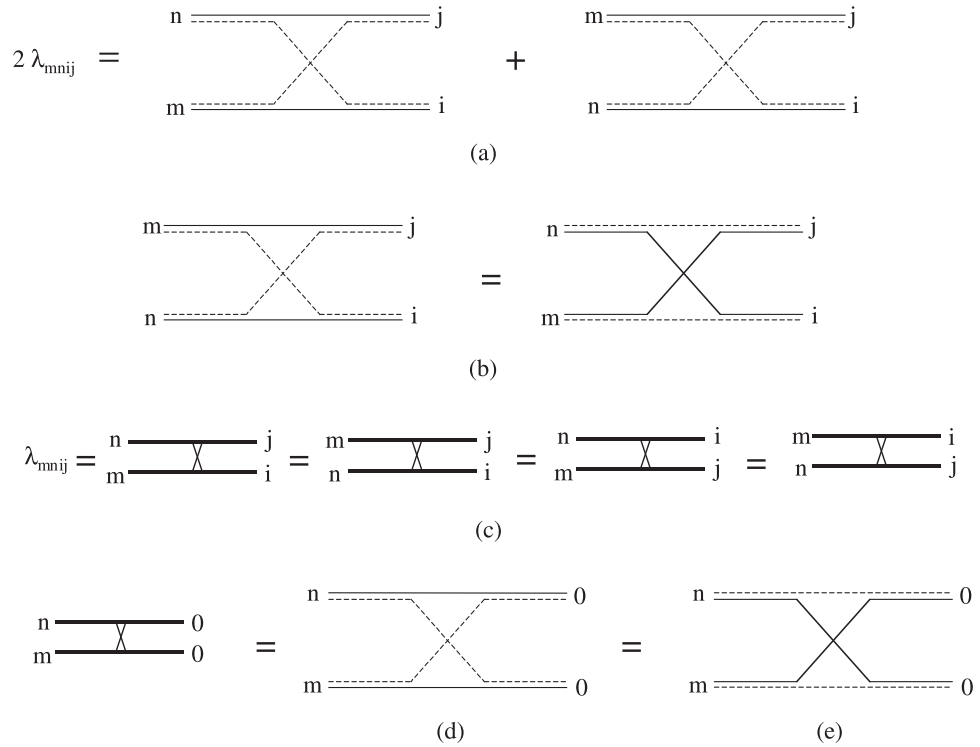

Fig. 1. Pauli scattering λ_{mnij} between the "in" excitons (i,j) and the "out" excitons (m,n). Solid line: electron; dashed line: hole; heavy solid line: exciton. (a): λ_{mnij}, defined in equation (3), is composed of two hole exchanges, in which the exciton indices (m,n) are inverted, so that $\lambda_{mnij} = \lambda_{nmij} = \lambda_{mnji}$. (b): A hole exchange between (i,j) leading to (n,m) corresponds to an electron exchange between (i,j) leading to (m,n). (c): In the "Pauli diagrams" of the following figures, the Pauli scattering λ_{mnij} will be represented by a cross. (d) and (e): When the two indices on one side are equal, the two processes of λ_{mnij} are identical: λ_{mn00} either corresponds to a hole exchange as in (d) or an electron exchange as in (e).

in the same state 0:

$$\langle v|B_{m_1}\cdots B_{m_n} B_0^{N-n}\, f(H)\, B_0^{\dagger N-n'} B_{i_1}^\dagger \cdots B_{i_{n'}}^\dagger|v\rangle. \quad (4)$$

These matrix elements can be calculated by "pushing" $f(H)$ to the right in order to end with $f(H)|v\rangle = f(0)|v\rangle$, if the vacuum energy is taken as zero. This push is done through a set of commutations. In the simplest case, $f(H) = H$, we have $HB_i^\dagger = B_i^\dagger(H + E_i) + V_i^\dagger$, which follows from $[H, B_i^\dagger] = E_i B_i^\dagger + V_i^\dagger$, the operator $V_i^\dagger$ being then pushed to the right, according to $[V_i^\dagger, B_j^\dagger] = \sum_{mn} \xi^{\rm dir}_{mnij} B_m^\dagger B_n^\dagger$, to end with $V_i^\dagger|v\rangle$ which is just 0. $\xi^{\rm dir}_{mnij}$, given by

$$\xi^{\rm dir}_{mnij} = \frac{1}{2}\int d\mathbf{r}_e\, d\mathbf{r}_{e'}\, d\mathbf{r}_h\, d\mathbf{r}_{h'}\, \phi_m^*(\mathbf{r}_e,\mathbf{r}_h)\, \phi_n^*(\mathbf{r}_{e'},\mathbf{r}_{h'}) \times (V_{ee'} + V_{hh'} - V_{eh'} - V_{e'h}) \times \phi_i(\mathbf{r}_e,\mathbf{r}_h)\phi_j(\mathbf{r}_{e'},\mathbf{r}_{h'}) \ + (m \leftrightarrow n), \quad (5)$$

is the other scattering of our many-body theory [2,3]. It corresponds to *direct* Coulomb processes, the "in" and "out" excitons being made with the same pairs — while, in λ_{mnij}, they have exchanged their carriers. Due to dimensional arguments, these $\xi^{\rm dir}_{mnij}$ for bound states are of the order of $R_X\mathcal{V}_X/\mathcal{V}$, with R_X being the exciton Rydberg [6].

Another $f(H)$ of interest is $1/(a-H)$, with a equal to $(\omega + i\eta)$ in problems involving photons. This $1/(a-H)$ is pushed to the right, according to [4]

$$\frac{1}{a-H}\, B_i^\dagger = B_i^\dagger\, \frac{1}{a-H-E_i} + \frac{1}{a-H}\, V_i^\dagger\, \frac{1}{a-H-E_i}, \quad (6)$$

which barely follows from $[H, B_i^\dagger]$. Due to dimensional arguments, this leads to an expansion in $\xi^{\rm dir}_{mnij}$ over an energy denominator which can be either a detuning or just an exciton energy difference, depending on the problem at hand.

A last $f(H)$ of interest is e^{-iHt}, as for problems dealing with time evolution. We can push it to the right according to [7]

$$e^{-iHt}\, B_i^\dagger = B_i^\dagger\, e^{-i(H+E_i)t} + W_i^\dagger(t), \quad (7)$$

$$W_i^\dagger(t) = -\int_{-\infty}^{+\infty} \frac{dx}{2i\pi}\, \frac{e^{-i(x+i\eta)t}}{x-H+i\eta}\, V_i^\dagger\, \frac{1}{x-H-E_i+i\eta}, \quad (8)$$

which follows from the integral representation of the exponential,

$$e^{-iHt} = -\int_{-\infty}^{+\infty} \frac{dx}{2i\pi}\, \frac{e^{-i(x+i\eta)t}}{x-H+i\eta}. \quad (9)$$

We see that, by passing $f(H)$ over $B_i^\dagger$, we essentially replace it by $f(H + E_i)$ — as if the exciton i were not

interacting with the other excitons — within a Coulomb term $V_i^\dagger$ which takes care of these interactions: $f(H+E_i)$ is, in some sense, the contribution of $f(H)$, in the absence of exciton interactions.

Once we have pushed all the H's up to $|v\rangle$ and generated very many Coulomb scatterings $\xi^{\rm dir}_{mnij}$, we end with scalar products of N-exciton states which look like equation (4) with $f(H)$ replaced by 1. We then start to push the B's to the right according to equations (1, 2), to end with $B|v\rangle = 0$. This set of pushes now makes appearing the Pauli scatterings λ_{mnij}.

For $N = 2$, equations (1, 2) readily give [2]

$$\langle v|B_m\, B_n\, B_i^\dagger\, B_j^\dagger|v\rangle = \delta_{mi}\,\delta_{nj} + \delta_{mj}\,\delta_{ni} - 2\lambda_{mnij}. \quad (10)$$

For large N however, a "brute force" calculation of N-exciton state scalar products is totally hopeless.

We expect these scalar products to depend on N and to contain very many λ_{mnij}'s. The amount of N they contain is actually of major importance: Indeed, physical quantities are expected to depend on N through $\eta = N\mathcal{V}_X/\mathcal{V}$, with possibly one extra N in front, for extensive quantities — the factors $\mathcal{V}_X/\mathcal{V}$ possibly coming from Pauli scatterings but also from Coulomb scatterings. However, as the scalar products of N-exciton states are not physical quantities in themselves, they can very well contain more complicated terms like $N^p\eta^n$ which have to ultimately disappear from the quantities of physical interest. To handle these various factors N properly — and prove the cancellation of the superextensive terms — is thus of major importance.

In previous works [1,5], we have studied the simplest of these scalar products of N-exciton states, namely $\langle v|B_0^N B_0^{\dagger N}|v\rangle$. We found it equal to $N!$, as for exact bosons, within a factor F_N,

$$\langle v|B_0^N\, B_0^{\dagger N}|v\rangle = N!\, F_N, \quad (11)$$

which behaves as $e^{-N\,O(\eta)}$ [5]. In large samples, $N\eta$ can be extremely large, even for η small, so that F_N can be exponentially small. In physical quantities however, this F_N does not appear alone, but through ratios like F_{N-p}/F_N which actually read as $1 + O(\eta)$ for $p \ll N$, so that these quantities end by depending on η only, as expected.

The present paper in fact deals with the interplay between the possible factors N and the various λ's which can appear in the scalar products of N-exciton states. These Pauli scatterings λ being the original part of our many-body theory for interacting composite bosons, the understanding of this interplay is actually fundamental to master many-body effects between composite excitons at any order in $\eta = N\mathcal{V}_X/\mathcal{V}$, — and also to cleanly show the exact cancellation of irrelevant superextensive terms, which can possibly appear at intermediate stages [7].

This paper is definitely formal. It however constitutes one very important piece of our many-body theory, because, in order to get any physical effect involving N interacting excitons, we ultimately end by having to calculate such scalar products. Problems involving two excitons only [7] are rather simple to handle, because they only use the scalar product of two-exciton states given in equation (10). The real challenge, which today remains to master many-body effects between N composite excitons at any order in η, is to produce the equivalent of equation (10) for large N.

In usual many-body effects, Feynman diagrams [8] have been proved to be quite convenient to understand the physics of interacting fermions or bosons. We expect the introduction of new diagrams appropriate to composite bosons, to also be quite convenient to understand the physics of their interactions. One important aspect of the present paper is in fact the study of these diagrams associated to possible carrier exchanges, starting from the so-called *"Pauli diagrams"* in which enter the Pauli scatterings between *two* excitons, as they appear when we use equations (1, 2). We will show that these Pauli diagrams turn out to be quite inappropriate, because diagrams appearing as very different can represent exactly the same quantity. To understand why these topologically different Pauli diagrams are in fact equivalent, is actually quite necessary if we want to master carrier exchanges between composite bosons. This will be done in the last section of the paper. The puzzling differences between these Pauli diagrams — that we saw as a signature of their impropriety to describe many-body effects between composite excitons —, led us to introduce the so-called *"skeleton diagrams"* and their associated "generalized carrier exchanges", i.e., *exchanges between more than two excitons*. Their appearance in a theory for composite bosons is actually fully reasonable because, Pauli exclusion being N-body "at once", when it plays a role, this Pauli exclusion correlates all the carriers of the excitons present, through a process which turns out to be quite complex — even if it is always possible to decompose it into a set of carrier exchanges between two excitons only, as in Pauli diagrams.

The possibility to describe carrier exchanges within Feynman diagrams, has been addressed by Strinati and coworkers [9,10]. The diagrams we here present are rather different because Pauli scatterings do not have their exact equivalent in Feynman diagrams: (i) These Pauli scatterings take care of boson statistics departure, while the fermion or boson statistics is included in the first lines of the usual many-body theories through the T-products of Green functions. (ii) These scatterings are formally equivalent to Coulomb scatterings, *except that they are dimensionless*. (iii) In the standard Feynman diagrams, exchange processes manifest themselves in the precise topology of the diagrams, the intermediate states in which the composite bosons are split, appearing explicitly through single-particle (bare) fermionic Green's functions (see Eqs. (2, 11) or (2, 15) of Ref. [10]). By contrast, in our skeleton exchange diagrams — which may look at first rather similar to the diagrams of Figure 2 of this reference [10] — the intermediate lines are just there to visualize how the "in" and "out" excitons are precisely constructed.

From a mathematical point of view, it is of course possible to calculate the scalar products of N-exciton states,

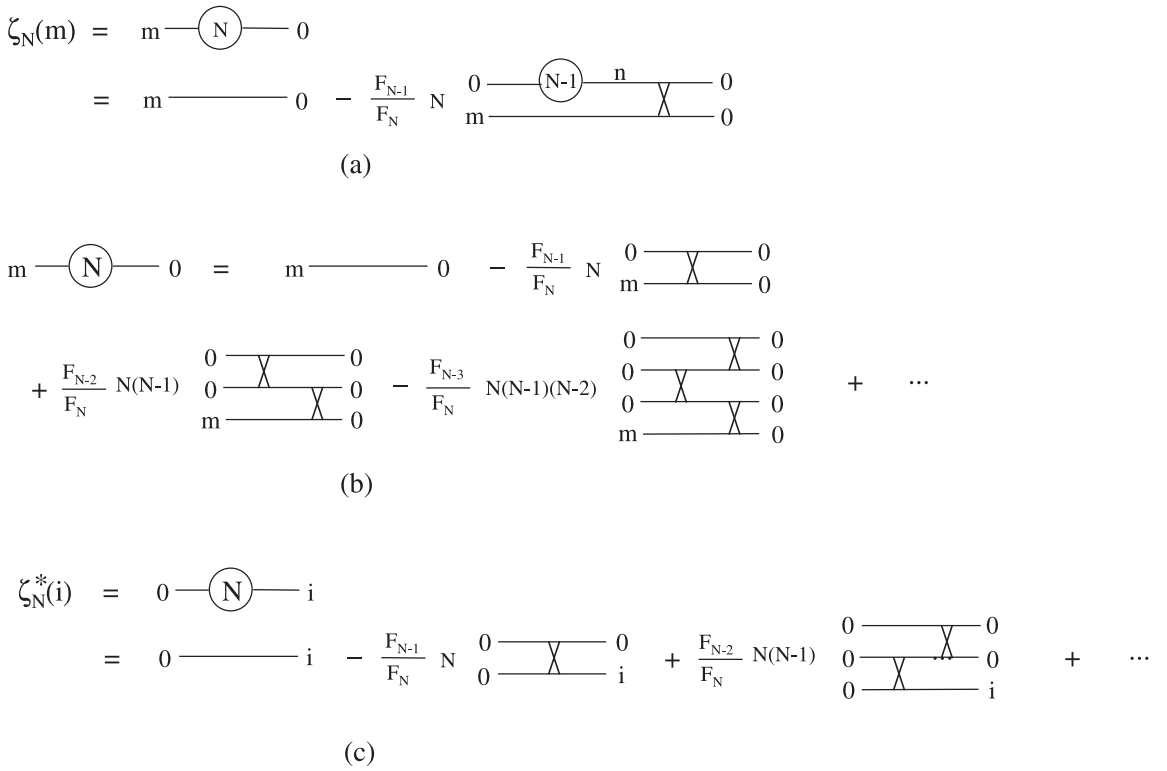

Fig. 2. (a): Recursion relation for the matrix element $\zeta_N(m)$ defined in equation (23). The $(m,0)$ line alone represents δ_{m0}, while the cross represents the Pauli scattering λ_{mn00}. Sum is taken over the intermediate exciton n. (b): Pauli diagrams for $\zeta_N(m)$ obtained by iteration of Figure 2a. They allow to visualize equation (25). Sums are taken over the (unlabelled) exciton lines. (c): The complex conjugate of $\zeta_N(i)$ is represented by similar zigzag diagrams, the relative position of the crosses being just changed.

just from blind algebra, and to get the right answer. However, in order to understand the appearance of extra factors N in front of the ones in $N\lambda \simeq N\mathcal{V}_X/\mathcal{V} = \eta$, crucial to ultimately withdraw superextensive terms from physical quantities, it is in fact convenient to introduce the concept of *"excitons dressed by a sea of excitons"*, because these extra factors N are physically linked to the underlying bosonic character of the excitons which is enhanced by the presence of a sea of excitons, all in the same state. We will show that these extra factors N are linked to the topology of the diagrams which represent these scalar products and which appear as "disconnected" when extra N's exist. This is after all not very surprising because disconnected Feynman diagrams are also known to produce superextensive terms.

Let us introduce these "excitons dressed by a sea of N excitons 0", defined as

$$|\psi_i^{(N)}\rangle = \frac{B_0^N B_0^{\dagger N}}{\langle v|B_0^N B_0^{\dagger N}|v\rangle}\, B_i^\dagger|v\rangle. \tag{12}$$

$\langle v|B_0^N B_0^{\dagger N}|v\rangle$ is a normalization factor which makes the operator in front of $B_i^\dagger$ appearing as an identity in the absence of Pauli interactions between the exciton i and the sea of excitons 0. For the vacuum state, dressed in the same way as

$$|\psi^{(N)}\rangle = \frac{B_0^N B_0^{\dagger N}}{\langle v|B_0^N B_0^{\dagger N}|v\rangle}\, |v\rangle, \tag{13}$$

we just find $|v\rangle$, as expected because no interaction can exist between the exciton sea and the vacuum. On the opposite, subtle Pauli interactions take place between the sea and an exciton i. By using the closure relation $1 = \sum_m B_m^\dagger|v\rangle\langle v|B_m$ for one-pair states, we can write this dressed exciton i as

$$|\psi_i^{(N)}\rangle = \sum_m A_N(m,i)\, B_m^\dagger|v\rangle, \tag{14}$$

$$A_N(m,i) = \frac{\langle v|B_m\, B_0^N\, B_0^{\dagger N}\, B_i^\dagger|v\rangle}{\langle v|B_0^N\, B_0^{\dagger N}|v\rangle}. \tag{15}$$

Since the physics which controls the extra N's, is actually linked to the underlying bosonic character of the excitons, let us first consider boson-excitons, in order to see how a sea of N boson-excitons 0 affects them.

2 Boson-excitons dressed by a sea of excitons

For boson-excitons, equation (1) is replaced by $[\bar{B}_m, \bar{B}_i^\dagger] = \delta_{mi}$, so that the deviation-from-boson operator D_{mi} is

zero, as well as all Pauli scatterings λ_{mnij}. From this boson commutator, we get by induction

$$[\bar{B}_0^N, \bar{B}_i^\dagger] = \bar{B}_0^{N-1}[\bar{B}_0, \bar{B}_i^\dagger] + [\bar{B}_0^{N-1}, \bar{B}_i^\dagger]\bar{B}_0 = N\delta_{0i}\,\bar{B}_0^{N-1}. \tag{16}$$

So that $\bar{B}_0^N \bar{B}_0^{\dagger N}|v\rangle = N!\,|v\rangle$, which shows that the normalization factor F_N is just 1. Consequently, $|\bar{\psi}_0^{(N)}\rangle$ defined as $|\psi_0^{(N)}\rangle$ with B_0 replaced by $\bar{B}_0$, is just $(N+1)\bar{B}_0^\dagger|v\rangle$ while $|\bar{\psi}_{i\neq 0}^{(N)}\rangle$ reduces to $\bar{B}_i^\dagger|v\rangle$. This leads to

$$|\bar{\psi}_i^{(N)}\rangle = (N\delta_{i0}+1)\,\bar{B}_i^\dagger|v\rangle. \tag{17}$$

The factor N which appears in this equation is nothing but the well known bosonic enhancement [11]. The memory of such an enhancement must a priori exist for composite bosons, such as the excitons. However, subtle changes are expected, due to their underlying fermionic character. Let us now see how this bosonic enhancement, obvious for boson-excitons, in fact appears for exact excitons.

3 Composite excitons dressed by a sea of excitons

From equations (1, 2), we easily get by induction

$$[D_{mi}, B_0^{\dagger N}] = 2N\sum_n \lambda_{mn0i}\,B_n^\dagger B_0^{\dagger N-1}, \tag{18}$$

$$[B_0^N, D_{mi}] = 2N\sum_j \lambda_{m0ji}\,B_0^{N-1}B_j, \tag{19}$$

since $D_{mi}^\dagger = D_{im}$, while $\lambda_{mnij}^* = \lambda_{ijmn}$. Equation (18) allows to generalize equation (1) as

$$[B_m, B_0^{\dagger N}] = NB_0^{\dagger N-1}(\delta_{m0} - D_{m0}) - N(N-1)\sum_n \lambda_{mn00}B_n^\dagger B_0^{\dagger N-2}, \tag{20}$$

$$[B_0^N, B_i^\dagger] = N(\delta_{0i} - D_{0i})B_0^{N-1} - N(N-1)\sum_j \lambda_{00ij}B_jB_0^{N-2}. \tag{21}$$

In order to grasp the origin of the bosonic enhancement which exists for composite excitons, let us start with the "best case" for such an enhancement, namely an exciton 0 dressed by a sea of N excitons 0.

3.1 Exciton 0 dressed by N excitons 0

From equation (14), this dressed exciton can be written as

$$|\psi_0^{(N)}\rangle = (N+1)\sum_m \zeta_N(m)B_m^\dagger|v\rangle \tag{22}$$

in which we have set

$$\zeta_N(m) = \frac{A_N(m,0)}{N+1} = \frac{\langle v|B_0^N B_m B_0^{\dagger N+1}|v\rangle}{(N+1)!F_N}. \tag{23}$$

This $\zeta_N(m)$, which is just $F_{N+1}/F_N \simeq 1+O(\eta)$ for $m=0$, will appear to be a quite useful quantity in the following. To calculate it, we use equation (20) for $B_mB_0^{\dagger N+1}$. Since $D_{m0}|v\rangle = 0$, which follows from equation (1) applied to $|v\rangle$, we readily get the following recursion relation for the $\zeta_N(m)$'s,

$$\zeta_N(m) = \delta_{m0} - \frac{F_{N-1}}{F_N}\,N\sum_n \lambda_{mn00}\,\zeta_{N-1}^*(n). \tag{24}$$

Its diagrammatic representation is shown in Figure 2a and its iteration in Figure 2b. The solution reads

$$\zeta_N(m) = \sum_{p=0}^{N}(-1)^p\frac{F_{N-p}}{F_N}\,\frac{N!}{(N-p)!}\,z^{(p)}(m,0), \tag{25}$$

with $z^{(0)}(m,0) = \delta_{m0}$, while

$$z^{(p)}(m,0) = \sum_n \lambda_{mn00}\,\left[z^{(p-1)}(n,0)\right]^* \tag{26}$$

is a zigzag diagram having $(p+1)$ exciton lines, the lowest one being $(m,0)$, while the p other lines are $(0,0)$. These lines are connected by p Pauli scatterings which are in zigzag, alternatively right, left, right... (see Fig. 2b). For $p=1$, $z^{(p)}(m,0)$ is just λ_{m000}, while for $p=2$, it reads $\sum_n \lambda_{mn00}\lambda_{00n0}$ and so on... Figure 2c also shows $\zeta_N^*(i)$, easy to obtain from $\zeta_N(m)$ by noting that $\lambda_{mnij}^* = \lambda_{ijmn}$, so that $\zeta_N^*(i)$ and $\zeta_N(i)$ are just related by a symmetry right-left, the zigzag being inverted.

Let us discuss the appearance of factors N in this $\zeta_N(m)$. If we forget about the exciton composite nature, we drop all carrier exchanges with the sea; the electron and hole are tight for ever as for boson-excitons, so that we should have the same result, $|\psi_0^{(N)}\rangle \simeq (N+1)B_0^\dagger|v\rangle$. This leads to $\zeta_N(m) \simeq \delta_{m0}$ at lowest order in carrier exchanges. Due to its composite nature, the exciton 0 can in fact exchange its electron, or its hole, with one sea exciton to become an exciton m. Since this sea exciton can be chosen among the N excitons of the sea, this first order exchange term must appear with a factor N in front. Another sea exciton, among the $(N-1)$ left, can also participate to these carrier exchanges; this makes the second order term in Pauli scattering appearing with a $N(N-1)$ prefactor; and so on...

$\zeta_N(m)$ thus contains the same number of factors N as the number of λ's. Since, for 0 and m being bound states, these λ's are in $\mathcal{V}_X/\mathcal{V}$, while F_{N-p}/F_N reads as an expansion in η (see Ref. [5]), $\zeta_N(m)$ ends by reading, in the large N limit, as an η expansion, without any extra factor N. This shows that $|\psi_0^{(N)}\rangle$, given in equation (22), contains the same bosonic enhancement factor $(N+1)$ as the one of the dressed boson-excitons $|\bar{\psi}_0^{(N)}\rangle$.

The relative weight $\zeta_N(0)$ of the $B_0^\dagger|v\rangle$ state in $|\psi_0^{(N)}\rangle$ — which is exactly 1 for boson-excitons —, is however smaller than 1 for composite excitons, due to possible carrier exchanges with the exciton sea. This weight in fact reads $\zeta_N(0) = 1 - (F_{N-1}/F_N)N\lambda_{0000} + \cdots$, which is nothing but F_{N+1}/F_N as can be directly seen from equation (23). This decrease of the weight of $|\psi_0^{(N)}\rangle$ on $B_0^\dagger|v\rangle$ is compensated by the non-zero components on $B_{m\neq 0}^\dagger|v\rangle$ — which do not exist for boson-excitons. Note that, since $\zeta_N(m) = 0$ for $\mathbf{Q}_m \neq \mathbf{Q}_0$, due to momentum conservation in Pauli scatterings, the other exciton states making $|\psi_0^{(N)}\rangle$ must have the same momentum $\mathbf{Q}_0$ as the 0 exciton one.

This leads us to conclude that the exciton 0 dressed by a sea of N excitons 0 exhibits the enhancement factor $(N+1)$ of boson-excitons. By contrast to boson-excitons, this dressed exciton however has components on excitons $i \neq 0$ having a momentum $\mathbf{Q}_i$ equal to the 0 exciton momentum $\mathbf{Q}_0$. Such a bosonic enhancement for the composite exciton 0 is somewhat normal because excitons are, after all, not so far from real bosons. We will now show that a similar enhancement also exists for excitons different from 0 but having a center of mass momentum equal to $\mathbf{Q}_0$. Before showing it from hard algebra, let us physically explain why this has to be so: From the two possible ways to form two excitons out of two electron-hole pairs, we have shown that [2,3]

$$B_i^\dagger B_j^\dagger = -\sum_{mn} \lambda_{mnij}\, B_m^\dagger B_n^\dagger. \tag{27}$$

$B_{i\neq 0}^\dagger B_0^\dagger$ can thus be written as a sum of $B_m^\dagger B_n^\dagger$'s with $\mathbf{Q}_m + \mathbf{Q}_n = \mathbf{Q}_i + \mathbf{Q}_0$ due to momentum conservation in the λ_{mnij} scatterings. For $\mathbf{Q}_i = \mathbf{Q}_0$, $B_{i\neq 0}^\dagger B_0^\dagger$ thus has a non-zero contribution on $B_0^{\dagger 2}$, so that this exciton $i \neq 0$, in the presence of other excitons 0, is partly an exciton 0: A bosonic enhancement has thus to exist for any exciton i with $\mathbf{Q}_i = \mathbf{Q}_0$.

3.2 Exciton i dressed by N excitons 0

We now consider an exciton with arbitrary i. There are essentially two kinds of such excitons, the ones with $\mathbf{Q}_i = \mathbf{Q}_0$ and the ones with $\mathbf{Q}_i \neq \mathbf{Q}_0$: Since a $\mathbf{Q}_i = \mathbf{Q}_0$ exciton can be transformed into an exciton $i = 0$ by carrier exchange with the exciton sea, the excitons with $\mathbf{Q}_i \neq \mathbf{Q}_0$ are in fact the only ones definitely different from excitons 0.

There are very many ways to calculate the component $A_N(m,i)$ defined in equation (15), for arbitrary excitons i and m: We can either start with $[B_m, B_i^\dagger]$ given in equation (1), or with $[B_m, B_0^{\dagger N}]$ given in equation (20), or even with $[B_0^N, B_i^\dagger]$ given in equation (21). While these last two ways lead to calculations essentially equivalent, the first one may appear somewhat better, because it does not destroy the intrinsic (m,i) symmetry of $A_N(m,i)$. These various ways to calculate $A_N(m,i)$ must of course end by giving exactly the same result. They however lead to diagrammatic representations of the scalar product $A_N(m,i)$ which are very different. In this section, we choose to calculate $A_N(m,i)$ in a way which leads to Pauli diagrams we find to have the "nicest" topology. The discussion of the other Pauli diagrams for $A_N(m,i)$ and the proof that they are topologically equivalent will be given in the last part of this work. This will lead us to introduce the skeleton diagrams which actually are the ones "behind" all these different Pauli diagrams.

3.2.1 Recursion relation between $A_N(m,i)$ and $A_{N-2}(n,i)$

To get this recursion relation, we start with $[B_m, B_i^\dagger]$ given in equation (1). This leads to

$$A_N(m,i) = a_N(m,i) + \hat{A}_N(i,m), \tag{28}$$

in which we have set

$$a_N(m,i) = \delta_{mi} - \langle v|B_0^N\, D_{mi}\, B_0^{\dagger N}|v\rangle/N!F_N, \tag{29}$$

$$\hat{A}_N(i,m) = \langle v|B_0^N B_i^\dagger B_m B_0^{\dagger N}|v\rangle/N!F_N. \tag{30}$$

To follow, we calculate $a_N(m,i)$, using $[D_{mi}, B_0^{\dagger N}]$ given in equation (18). This leads to

$$a_N(m,i) = \delta_{mi} - 2\frac{F_{N-1}}{F_N}\, N \sum_j \lambda_{mj0i}\, \zeta_{N-1}^*(j), \tag{31}$$

which is shown in Figure 3a, Figure 3b being the corresponding expansion of $a_N(m,i)$ obtained by using $\zeta_N^*(i)$ given in Figure 2c. By injecting equation (25) into equation (31), this $a_N(m,i)$ reads

$$a_N(m,i) = \delta_{mi} + 2\sum_{p=1}^{N}(-1)^p\, \frac{F_{N-p}}{F_N}\, \frac{N!}{(N-p)!}\, z^{(p)}(m,i), \tag{32}$$

where $z^{(p)}(m,i)$ is a zigzag diagram like $z^{(p)}(m,0)$, with the lowest line $(m,0)$ replaced by (m,i), see Figure 3b. It is such that

$$z^{(p)}(m,i) = \sum_j \lambda_{mj0i}\, \left[z^{(p-1)}(j,0)\right]^*. \tag{33}$$

If we now turn to $\hat{A}_N(i,m)$, given in equation (30), in order to write it in terms of $A_{N-2}(n,i)$, we use $[B_m, B_0^{\dagger N}]$. This leads to

$$\hat{A}_N(i,m) = \frac{F_{N-1}}{F_N}\, N\, \delta_{m0}\, \zeta_{N-1}^*(i) - \frac{N(N-1)}{N!F_N} \sum_j \lambda_{mj00}\, \langle v|B_0^N B_i^\dagger B_j^\dagger B_0^{\dagger N-2}|v\rangle. \tag{34}$$

So that, using $[B_0^N, B_j^\dagger]$, we end with

$$\hat{A}_N(i,m) = N\, b_N(m,i) + \frac{F_{N-2}}{F_N}\, N(N-1) \sum_{nj} \lambda_{mj00}\lambda_{00nj}\, A_{N-2}(n,i), \tag{35}$$

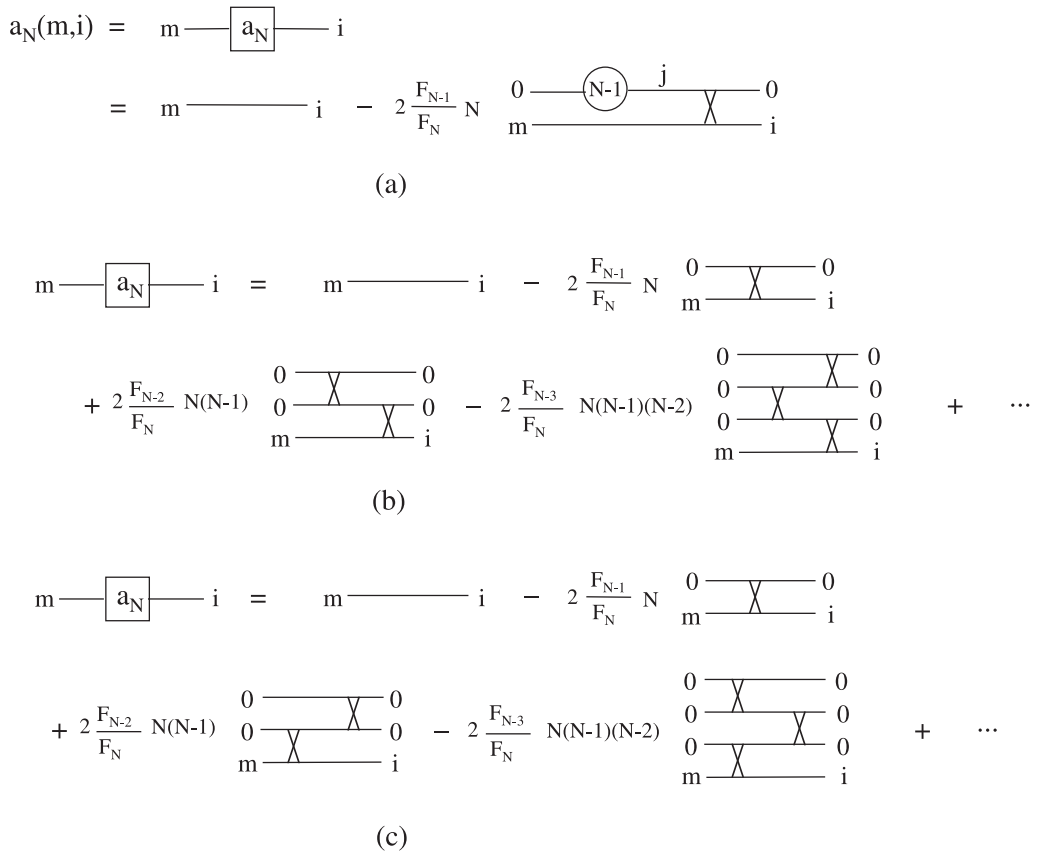

Fig. 3. (a): Diagrammatic representation of equation (31) for $a_N(m,i)$ defined in equation (29). (b): Pauli diagrams for $a_N(m,i)$, obtained by inserting the diagrams of Figure 2c for ζ^* into Figure 3a. They contain 0, 1, 2, 3, ... Pauli scatterings represented by crosses, put in zigzag, alternatively right, left, right, ..., m and i staying on the bottom line. Figure 3b is just a visualization of equation (32). Here again, as in all Pauli diagrams, sums are taken over the intermediate (unlabelled) exciton lines. (c): Other diagrammatic representation of the same $a_N(m,i)$ obtained by using $[B_0^N, D_{mi}]$, instead of $[D_{mi}, B_0^{\dagger N}]$, in equation (29).

in which we have set

$$b_N(m,i) = \frac{F_{N-1}}{F_N}\,\delta_{m0}\,\zeta^*_{N-1}(i) - \frac{F_{N-2}}{F_N}\,(N-1)\,\lambda_{m000}\,\zeta^*_{N-2}(i)$$

$$= \frac{F_{N-1}}{F_N}\,\delta_{m0}\,\delta_{0i} + \sum_{p=1}^{N-1}(-1)^p\,\frac{(N-1)!}{(N-1-p)!}\,\frac{F_{N-1-p}}{F_N} \times \left\{ z^{(0)}(m,0)\,\left[z^{(p)}(i,0)\right]^* + z^{(1)}(m,0)\,\left[z^{(p-1)}(i,0)\right]^* \right\}, \quad (36)$$

due to equation (25) for $\zeta_N(m)$.

The diagrammatic representations of equations (36) are shown in Figure 4. From Figure 4a, which represents the first line of equation (36), and the diagrams of Figure 2c for $\zeta^*_N(i)$, we obtain the Pauli expansion of $b_N(m,i)$ shown in Figure 4b. We see that the diagrams for $b_N(m,i)$ are made of two parts. We also see that, while $a_N(m,i)$ differs from 0 for $\mathbf{Q}_m = \mathbf{Q}_i$ only (due to momentum conservation included in the Pauli scatterings), we must have $\mathbf{Q}_m = \mathbf{Q}_i = \mathbf{Q}_0$ for $b_N(m,i)$ to differ from zero, since $\zeta_N(m)$ is zero for $\mathbf{Q}_m \neq \mathbf{Q}_0$, as previously shown.

Using equations (28) and (35), we end with a recursion relation for $A_N(m,i)$ which reads

$$A_N(m,i) = a_N(m,i) + N\,b_N(m,i) + \frac{F_{N-2}}{F_N}\,N(N-1)\sum_{nj}\lambda_{mj00}\lambda_{00nj}\,A_{N-2}(n,i). \quad (37)$$

3.2.2 Determination of $A_N(m,i)$ using $A_{N-2}(n,i)$

As $a_N(m,i) \neq 0$ for $\mathbf{Q}_m = \mathbf{Q}_i$, while $b_N(m,i) \neq 0$ imposes $\mathbf{Q}_m = \mathbf{Q}_i = \mathbf{Q}_0$, we divide $A_N(m,i)$ into a contribution which exists whatever $\mathbf{Q}_i$ is and a contribution which only

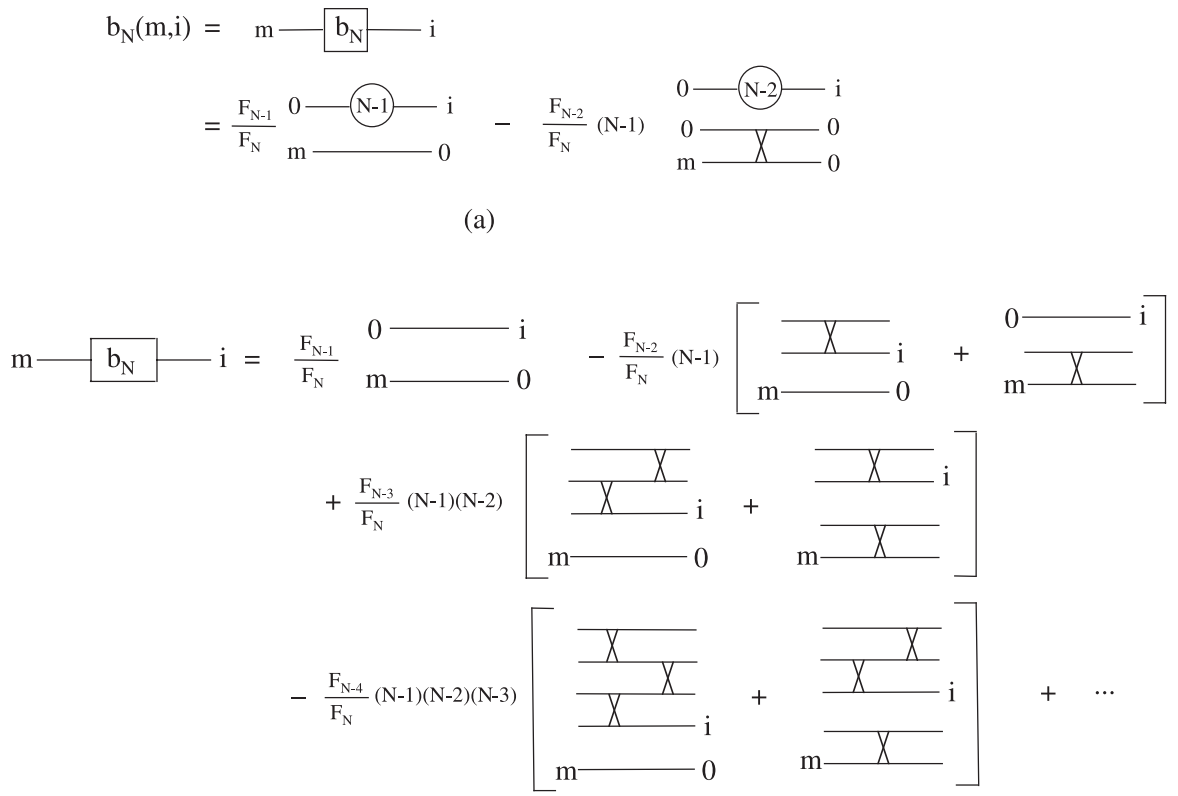

Fig. 4. (a): Diagrammatic representation of $b_N(m,i)$ given by the first equation (36). (b): Pauli diagrams for $b_N(m,i)$, obtained by inserting the diagrams of Figure 2c for ζ^* into Figure 4a. $b_N(m,i)$ is made of a set of *disconnected* diagrams, with 0, 1, 2, 3, ... Pauli scatterings. One part always has a δ_{m0} factor, the other part having a λ_{m000} factor, which makes the roles played by (m,i) dissymetrical. The omitted exciton indices at the end of the lines, are always 0. Figure 4b is a simple visualization of the second equation (36).

exists when $\mathbf{Q}_i$ is equal to the sea exciton momentum $\mathbf{Q}_0$. This leads to

$$A_N(m,i) = \alpha_N(m,i) + N\,\beta_N(m,i), \tag{38}$$

where $\alpha_N(m,i)$ and $\beta_N(m,i)$ now obey

$$\alpha_N(m,i) = a_N(m,i) + \frac{F_{N-2}}{F_N}\,N(N-1)\sum_{nj}\lambda_{mj00}\lambda_{00nj}\,\alpha_{N-2}(n,i), \tag{39}$$

$$\beta_N(m,i) = b_N(m,i) + \frac{F_{N-2}}{F_N}\,(N-1)(N-2)\sum_{nj}\lambda_{mj00}\lambda_{00nj}\,\beta_{N-2}(n,i). \tag{40}$$

a) Part of $A_N(m,i)$ which exists whatever $\mathbf{Q}_i(=\mathbf{Q}_m)$ is

The part of $A_N(m,i)$ which exists for any exciton i is $\alpha_N(m,i)$. Its diagrammatic representation, obtained from the iteration of the recursion relation (39), is shown in Figure 5. (In order to get rid of the 2 appearing in $a_N(m,i)$, we have used $\lambda_{mn0i} = \lambda_{mni0}$.) Equation (32) for $a_N(m,i)$ leads to write the solution of equation (39) as

$$\alpha_N(m,i) = \sum_{p=0}^{N}(-1)^p\,\frac{F_{N-p}}{F_N}\,\frac{N!}{(N-p)!}\,Z^{(p)}(m,i), \tag{41}$$

where $Z^{(p)}(m,i)$ obeys the recursion relation

$$Z^{(p)}(m,i) = \hat{z}^{(p)}(m,i) + \sum_{nj}\lambda_{mj00}\,\lambda_{00nj}\,Z^{(p-2)}(n,i), \tag{42}$$

with $\hat{z}^{(0)} = \delta_{mi}$, while $\hat{z}^{(p\neq 0)}(m,i) = 2z^{(p)}(m,i)$. As shows Figure 5, $Z^{(p)}(m,i)$ is represented by a sum of zigzag diagrams with p Pauli scatterings alternatively right, left, right, ..., the index m being always at the left bottom, while i can be at all possible places on the right. $Z^{(p)}(m,i)$ thus contains $(p+1)$ diagrams which reduce to one, namely $Z^{(0)}(m,i) = \delta_{mi}$, when $p = 0$.

From Figure 5 we also see that $\alpha_N(m,i)$ contains as many N's as λ's so that it ultimately depends on (N,λ)'s through η only.

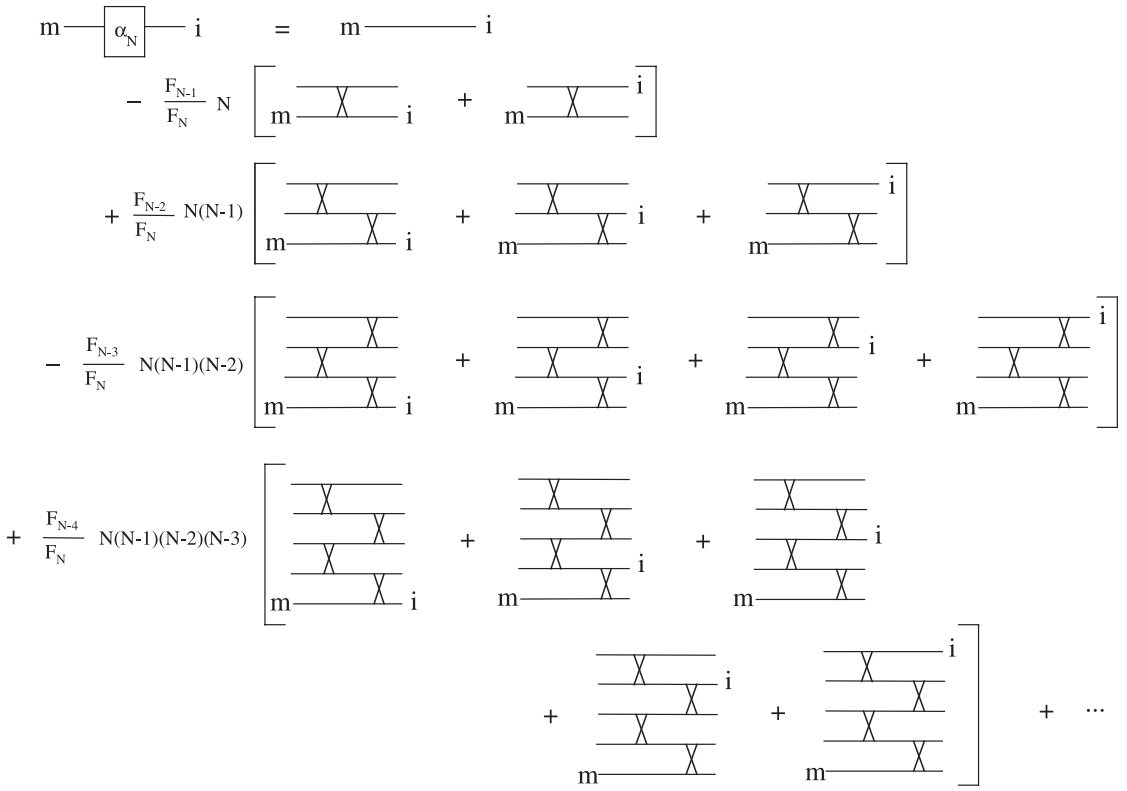

Fig. 5. Pauli diagrams for the part $\alpha_N(m,i)$ of the scalar product $A_N(m,i)$ which exists even if $\mathbf{Q}_m = \mathbf{Q}_i \neq \mathbf{Q}_0$ as obtained from the recursion relation (39). They are made of zigzag diagrams with Pauli scatterings put alternatively right, left, right, ..., the index m staying at the left bottom, while i runs in all possible positions on the right. This figure is a simple visualization of equation (41).

b) Part of $A_N(m,i)$ which exists for $\mathbf{Q}_i(=\mathbf{Q}_m) = \mathbf{Q}_0$ only

The part of $A_N(m,i)$ which only exists when the excitons i and m have the sea exciton momentum, is $N\,\beta_N(m,i)$. The diagrammatic representation obtained from the iteration of the recursion relation (40) for β_N is shown in Figure 6. Using equations (26, 36), its solution reads

$$\beta_N(m,i) = \sum_{p=0}^{N-1} (-1)^p \, \frac{F_{N-1-p}}{F_N} \, \frac{(N-1)!}{(N-1-p)!} \times \sum_{q=0}^{p} z^{(q)}(m,0)\, z^{(p-q)*}(i,0), \quad (43)$$

which just corresponds to the diagrams of Figure 6. These diagrams are made of two parts. We also see that $\beta_N(m,i)$ contains as many N's as λ's so that $\beta_N(m,i)$, like $\alpha_N(m,i)$, is an η function.

c) N dependence of $A_N(m,i)$

If we now come back to the expression (38) for $A_N(m,i)$, we see that, when $\mathbf{Q}_m = \mathbf{Q}_i \neq \mathbf{Q}_0$, $\beta_N(m,i) = 0$, so that the N's in $A_N(m,i)$ simply appear through the η's of $\alpha_N(m,i)$. On the opposite, $A_N(m,i)$ contains an extra prefactor N when $\beta_N(m,i) \neq 0$, i.e., when $\mathbf{Q}_m = \mathbf{Q}_i = \mathbf{Q}_0$: This extra N is the memory of the bosonic enhancement found for the dressed exciton $i = 0$, which also exists for an exciton i convertible into an exciton 0 by Pauli scatterings with the sea excitons, i.e., an exciton with $\mathbf{Q}_i = \mathbf{Q}_0$.

From a mathematical point of view, this extra N is linked to the topology of the diagrams representing $A_N(m,i)$. As in standard Feynman diagrams for which superextensive terms are linked to disconnected processes, we here see that an extra factor N appears in the part of $A_N(m,i)$ corresponding to diagrams which are made of two parts.

To conclude, we can say that the procedure used here to calculate $A_N(m,i)$ leads to Pauli diagrams which are actually quite simple: The part of $A_N(m,i)$ which exists for any $\mathbf{Q}_m = \mathbf{Q}_i$, is made of all connected diagrams with m at the left bottom and i at all possible places on the right, the exciton lines being connected by Pauli scatterings put in zigzag right, left, right... (see Fig. 5). $A_N(m,i)$ has an additional part when the excitons m and i have a momentum equal to the sea exciton momentum $\mathbf{Q}_0$. This additional part is made of all possible Pauli diagrams made of two parts, m staying at the left bottom of one part, while i stays at the right bottom of the other part, the exciton lines being connected by Pauli scatterings in zigzag right, left, right... for the m part, and left, right, left... for the i part (see Fig. 6). As a direct consequence of the topology of these disconnected diagrams, an

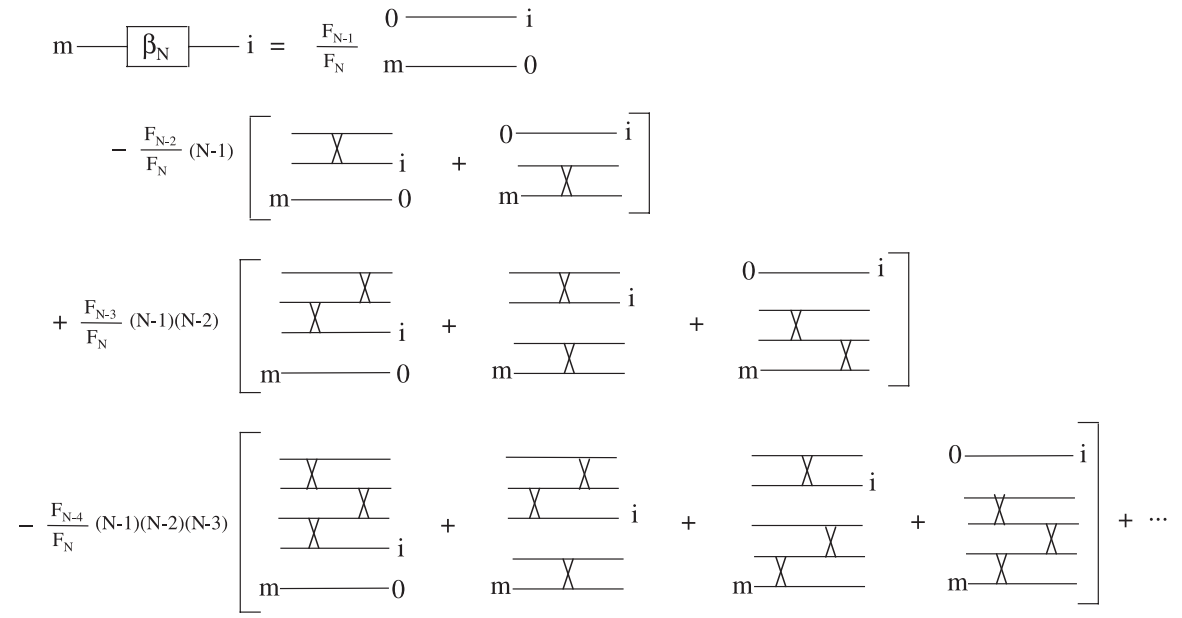

Fig. 6. Pauli diagrams for the part $\beta_N(m,i)$ of the scalar product $A_N(m,i)$ which exists for $\mathbf{Q}_m = \mathbf{Q}_i = \mathbf{Q}_0$ only, as obtained from the iteration of the recursion relation (40). $\beta_N(m,i)$ is made of *disconnected* diagrams, the two parts being zigzag diagrams right, left, right, ... for the part with m at the left bottom, and left, right, left, ... for the part with i at the right bottom. This figure is a simple visualization of equation (43).

extra factor N then appears in $A_N(m,i)$. This factor N is physically linked to the well known bosonic enhancement which, for composite excitons, exists not only for an exciton identical to a sea exciton, but also for any exciton which can be transformed into a sea exciton by Pauli scatterings with the sea.

Although this result for the scalar product of $(N+1)$-exciton states, with N of them in the same state 0, is nicely simple at any order in Pauli interaction, it does not leave us completely happy. Indeed, while, in the disconnected diagrams the m and i indices play similar roles, their roles in the diagrams which exist even if $\mathbf{Q}_i \neq \mathbf{Q}_0$, are dissymmetric, which is not at all satisfactory since $A_N(m,i) = [A_N(i,m)]^*$. This dissymmetry can be traced back to the way we have calculated $A_N(m,i)$. It is clear that equivalences between Pauli diagrams must exist in order to restore the intrinsic (m,i) symmetry of $A_N(m,i)$. In the next part, we are going to derive some equivalent Pauli diagrams for $A_N(m,i)$. This will lead us to identify the intrinsic exchange structure between N excitons which exists "behind" these Pauli diagrams, namely the skeleton diagrams. These skeleton diagrams, presented in the last part of this work, are in fact the appropriate diagrams for the exchange part of our many-body theory for interacting excitons.

4 Other Pauli diagrams for $\mathbf{A_N(m,i)}$

In order to have some ideas on which kinds of Pauli diagrams can be equivalent, let us first derive two other diagrammatic representations of $A_N(m,i)$ based on recursion relations between $A_N(m,i)$ and $A_{N-2}(m,j)$, or $A_{N-2}(n,j)$, instead of $A_{N-2}(n,i)$.

4.1 Pauli diagrams using $\mathbf{A_{N-2}(m,j)}$

To get this recursion relation, we must keep B_m in the calculation of $\hat{A}_N(m,i)$ defined in equation (30). For that, we use $[B_0^N, B_i^\dagger]$ instead of $[B_m, B_0^{\dagger N}]$; equation (35) is then replaced by

$$\hat{A}_N(m,i) = N\, c_N(m,i) + \frac{F_{N-2}}{F_N}\, N(N-1) \sum_{nj} \lambda_{nj00}\, \lambda_{00in}\, A_{N-2}(m,j), \quad (44)$$

in which we have set

$$c_N(m,i) = \frac{F_{N-1}}{F_N}\, \delta_{0i}\, \zeta_{N-1}(m) - \frac{F_{N-2}}{F_N}\, (N-1) \lambda_{000i}\, \zeta_{N-2}(m). \quad (45)$$

Using Figure 2b for $\zeta_N(m)$, we get the diagrams for $c_N(m,i)$ shown in Figure 7. When compared to $b_N(m,i)$, we see that the roles played by m and i are exchanged as well as the relative position of the crosses.

Equation (44) leads to write $A_N(m,i)$ given in equation (28) as

$$A_N(m,i) = \overline{\alpha}_N(m,i) + N\, \overline{\beta}_N(m,i), \quad (46)$$

where $\overline{\alpha}_N(m,i)$ and $\overline{\beta}_N(m,i)$ now obey

$$\overline{\alpha}_N(m,i) = a_N(m,i) + \frac{F_{N-2}}{F_N}\, N(N-1) \sum_{nj} \lambda_{nj00}\, \lambda_{00in}\, \overline{\alpha}_{N-2}(m,j), \quad (47)$$

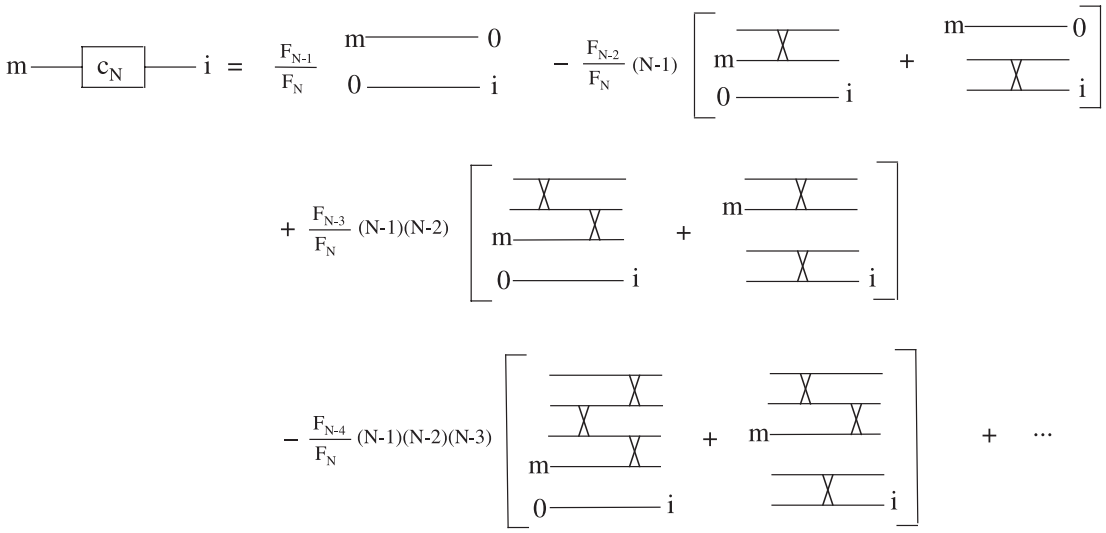

Fig. 7. Pauli diagrams for $c_N(m,i)$ defined in equation (45). This $c_N(m,i)$ appears instead of $b_N(m,i)$ when $A_N(m,i)$ is written in terms of $A_{N-2}(m,j)$ instead of $A_{N-2}(n,i)$. As $b_N(m,i)$, $c_N(m,i)$ is made of disconnected diagrams. At each order, it contains two terms, one with a δ_{i0} factor, the other with a λ_{000i} factor.

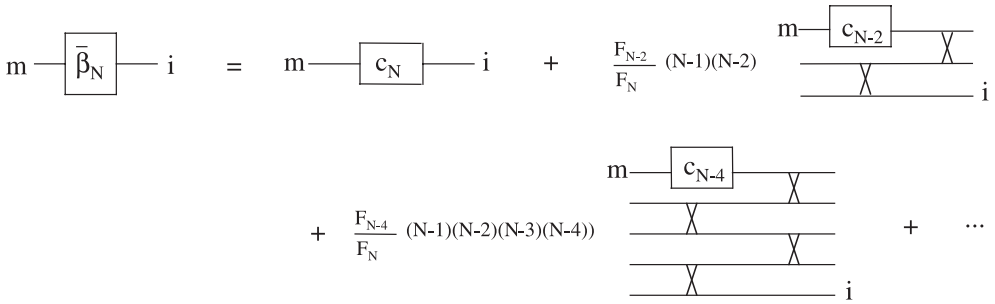

Fig. 8. Diagrammatic representation of the $\overline{\beta}_N(m,i)$ part of $A_N(m,i)$ which exists for $\mathbf{Q}_m = \mathbf{Q}_i = \mathbf{Q}_0$ only, as it appears when we use the recursion relation between $A_N(m,i)$ and $A_{N-2}(m,j)$, instead of $A_{N-2}(n,i)$. This diagrammatic representation corresponds to the iteration of equation (48). By inserting the diagrams for $c_N(m,i)$, shown in Figure 7, in this Figure 8, it is straightforward to see that the Pauli diagrams for $\overline{\beta}_N(m,i)$ are identical to the ones for $\beta_N(m,i)$ shown in Figure 6, at any order in Pauli scatterings, so that $\overline{\beta}_N(m,i) = \beta_N(m,i)$.

$$\overline{\beta}_N(m,i) = c_N(m,i) + \frac{F_{N-2}}{F_N}(N-1)(N-2)\sum_{nj}\lambda_{nj00}\,\lambda_{00in}\,\overline{\beta}_{N-2}(m,j). \tag{48}$$

$\overline{\beta}_N(m,i)$, as $\beta_N(m,i)$, differs from zero for $\mathbf{Q}_m = \mathbf{Q}_i = \mathbf{Q}_0$ only. Its recursion relation leads to expand it in terms of c_{N-p}'s as shown in Figure 8. Using for these c_{N-p}'s the expansion shown in Figure 7, we immediately find that $\overline{\beta}_N(m,i)$ is represented by the *same* Pauli diagrams as the ones for $\beta_N(m,i)$, so that $\overline{\beta}_N(m,i) = \beta_N(m,i)$. This is after all not surprising because, in them, the roles played by m and i are symmetrical. From this result, we conclude that the parts of $A_N(m,i)$ which exist even if $\mathbf{Q}_i = \mathbf{Q}_m \neq \mathbf{Q}_0$ have also to be equal, i.e., we must have $\overline{\alpha}_N(m,i) = \alpha_N(m,i)$.

If we now calculate $a_N(m,i)$ not with $[D_{mi}, B_0^{\dagger N}]$ but with $[B_0^N, D_{mi}]$, we find that $a_N(m,i)$ can also be represented by the diagrams of Figure 3c. These diagrams look very similar to the ones of Figure 3b, except that the crosses are now in zigzag left, right, left... Since the sets of diagrams (3b) and (3c) represent the same quantity $a_N(m,i)$, while they have to be valid for $N = 2, 3, \cdots$, we conclude that the relative positions of the crosses must be unimportant in these Pauli diagrams. We will prove this equivalence in Section 5.

The iteration of the recursion relation for $\overline{\alpha}_N(m,i)$ leads to the diagrams of Figure 9. They look like the ones for $\alpha_N(m,i)$, except that i now stays at the right bottom while m moves to all possible positions on the left, the zigzag for the Pauli scatterings being now left, right, left... This leads to write $\overline{\alpha}_N(m,i)$ as

$$\overline{\alpha}_N(m,i) = \sum_{p=0}^{N}(-1)^p\,\frac{F_{N-p}}{F_N}\,\frac{N!}{(N-p)!}\,\overline{Z}^{(p)}(m,i), \tag{49}$$

where $\overline{Z}^{(p)}(m,i)$ represents the set of zigzag diagrams of Figure 9 containing p crosses.

Since $\overline{\alpha}_N(m,i) = \alpha_N(m,i)$, we conclude from the expansions of these two quantities for $N = 2, 3, \cdots$, that

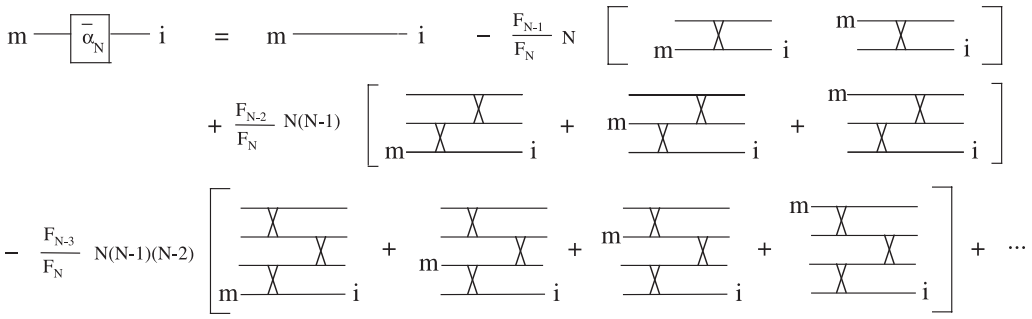

Fig. 9. Diagrammatic expansion of the $\overline{\alpha}_N(m,i)$ part of $A_N(m,i)$ which exists even if $\mathbf{Q}_m = \mathbf{Q}_i \neq \mathbf{Q}_0$, as it appears from the iteration of the recursion relation between $A_N(m,i)$ and $A_{N-2}(m,j)$. These Pauli diagrams look like the ones for $\alpha_N(m,i)$, shown in Figure 5, except for positions of the zigzags which are now left, right, left, ..., with i staying at the right bottom and m moving at all possible positions on the left. Since $\overline{\beta}_N(m,i) = \beta_N(m,i)$, we have $\overline{\alpha}_N(m,i) = \alpha_N(m,i)$ for any N; so that these Pauli diagrams for $\overline{\alpha}_N(m,i)$ and the ones for $\alpha_N(m,i)$ shown in Figure 5, must correspond to the same quantity, at any order in Pauli scatterings. This will be proved later on.

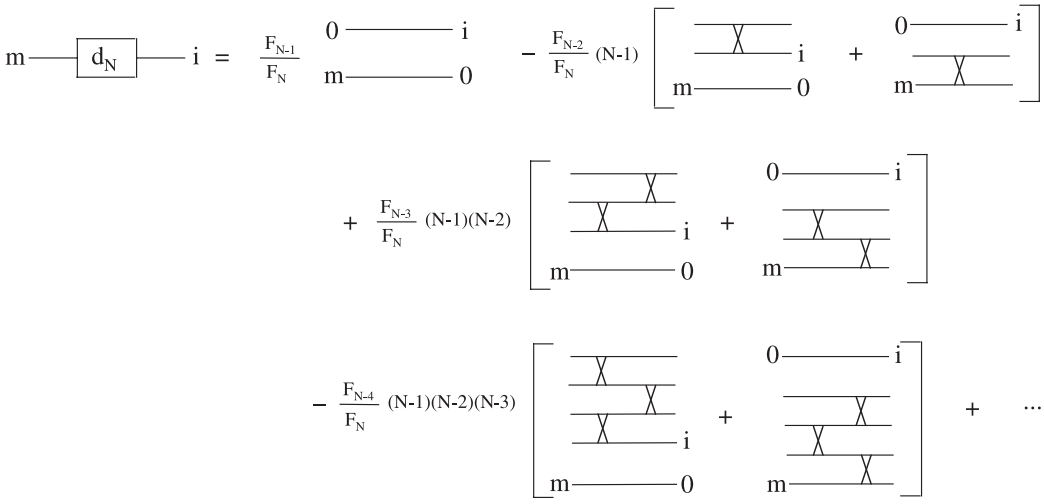

Fig. 10. Pauli diagrams for $d_N(m,i)$ defined in equation (51). This $d_N(m,i)$ is the quantity which appears instead of $b_N(m,i)$ when we write $A_N(m,i)$ in terms of $A_{N-2}(n,j)$ and not in terms of $A_{N-2}(n,i)$. As $b_N(m,i)$, $d_N(m,i)$ is made of disconnected diagrams, with two parts at each order, one having a δ_{m0} factor, the other a δ_{0i} factor.

the zigzag diagrams $Z^{(p)}(m,i)$ and $\overline{Z}^{(p)}(m,i)$ must correspond to the same quantity, for any p.

4.2 Pauli diagrams using $\mathbf{A_{N-2}(n,j)}$

To get this recursion relation, we start as for the one between $A_N(m,i)$ and $A_{N-2}(n,i)$, but we use $[B_0^N, B_i^\dagger]$ instead of $[B_0^N, B_j^\dagger]$. This leads to

$$\hat{A}_N(m,i) = N\, d_N(m,i) + \frac{F_{N-2}}{F_N}\, N(N-1) \sum_{nj} \lambda_{mj00}\, \lambda_{00ni}\, A_{N-2}(n,j), \tag{50}$$

in which we have set

$$d_N(m,i) = \frac{F_{N-1}}{F_N}\, \delta_{m0}\, \zeta^*_{N-1}(i) - \frac{F_{N-2}}{F_N}\, (N-1)\, \delta_{0i} \sum_j \lambda_{mj00}\, \zeta^*_{N-2}(j). \tag{51}$$

Using the diagrams of Figure 2c for $\zeta^*_N(i)$, we find that $d_N(m,i)$ is represented by the diagrams of Figure 10. Note that $d_N(m,i)$ is equal to zero when both $m \neq 0$ and $i \neq 0$, while, for $b_N(m,i)$ and $c_N(m,i)$, we just need $\mathbf{Q}_m = \mathbf{Q}_i \neq \mathbf{Q}_0$.

Equation (50) leads to write $A_N(m,i)$ as

$$A_N(m,i) = \overline{\overline{\alpha}}_N(m,i) + N\, \overline{\overline{\beta}}_N(m,i), \tag{52}$$

where $\overline{\overline{\alpha}}_N(m,i)$ and $\overline{\overline{\beta}}_N(m,i)$ now obey

$$\overline{\overline{\alpha}}_N(m,i) = a_N(m,i) + \frac{F_{N-2}}{F_N} N(N-1) \sum_{nj} \lambda_{mj00}\, \lambda_{00ni}\, \overline{\overline{\alpha}}_{N-2}(n,j), \tag{53}$$

$$\overline{\overline{\beta}}_N(m,i) = d_N(m,i) + \frac{F_{N-2}}{F_N}(N-1)(N-2) \sum_{nj} \lambda_{mj00}\, \lambda_{00ni}\, \overline{\overline{\beta}}_{N-2}(n,j). \tag{54}$$

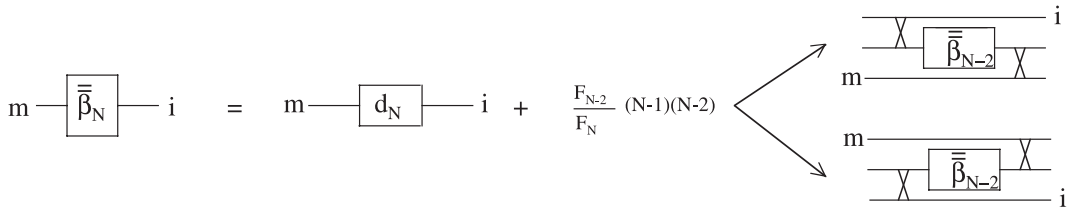

Fig. 11. (a): The two possible representations of the same recursion relation (54) for the $\overline{\overline{\beta}}_N(m,i)$ part of $A_N(m,i)$ which exists for $\mathbf{Q}_m = \mathbf{Q}_i = \mathbf{Q}_0$ only, as they appear when we use the recursion relation between $A_N(m,i)$ and $A_{N-2}(n,j)$ instead of $A_{N-2}(n,i)$. These two representations just result from an up-down symmetry which follows from Figure 1c, since $\lambda_{mnij} = \lambda_{nmji}$. (b): Iteration of this recursion relation. The two representations of $\overline{\overline{\beta}}_N(m,i)$ shown in Figure 11a have been alternatively used in order to avoid the crossings of the exciton lines. By inserting in this Figure 11b the diagrams of Figure 10 for $d_N(m,i)$, we see that the Pauli diagrams for $\overline{\overline{\beta}}_N(m,i)$ are exactly those of $\beta_N(m,i)$ shown in Figure 6, so that $\overline{\overline{\beta}}_N(m,i) = \beta_N(m,i)$.

The recursion relation for $\overline{\overline{\beta}}_N(m,i)$ is shown in Figure 11a and its iteration in Figure 11b. (In it, we have used the two equivalent forms of this recursion relation given in Fig. 11a.) If, in these diagrams, we now insert the diagrammatic representation of $d_N(m,i)$ shown in Figure 10, with the m part alternatively below and above the i part, we find that $\overline{\overline{\beta}}_N(m,i)$ is represented by exactly the same diagrams as the ones for $\beta_N(m,i)$, so that $\overline{\overline{\beta}}_N(m,i) = \beta_N(m,i)$. As a consequence, we must have $\overline{\overline{\alpha}}_N(m,i) = \alpha_N(m,i)$.

Let us now consider $\overline{\overline{\alpha}}_N(m,i)$. The iteration of the recursion relation (53) leads to the diagrams of Figure 12a. If in it, we insert the diagrammatic representation of $a_N(m,i)$ shown in Figure 3b, we get the diagrams of Figure 12b. Let us stress that it is not enough to use $\lambda_{0n00} = \lambda_{n000}$ to transform the last third order diagram of this Figure 12b into the two last third order zigzag diagrams, left, right, left, ..., of $\alpha_N(m,i)$. The situation is even worse for the last fourth order diagram of $\overline{\overline{\alpha}}_N(m,i)$ which is totally different from a zigzag diagram. These diagrams however have to represent the same quantity at any order in Pauli scatterings, since, for any N, we have $\overline{\overline{\alpha}}_N(m,i) = \alpha_N(m,i)$.

Let us now identify the underlying reason for the equivalence of Pauli diagrams like the ones of Figures 3b and 3c which represent $a_N(m,i)$, or the ones of Figures 5, 9, 12b which represent the part of $A_N(m,i)$ which exists even if $\mathbf{Q}_m (= \mathbf{Q}_i) \neq \mathbf{Q}_0$. This will help us to understand how these Pauli diagrams really work, and to pick out the generic diagrams which are "behind" them.

5 Skeleton diagrams

All the Pauli diagrams we found in the preceding sections, are made of a certain number of exciton lines connected by Pauli scatterings between two excitons, put in various positions. It is clear that the value of these diagrams has to depend on the "in" and "out" exciton states, i.e., the indices which appear at the right and the left of these diagrams, but not on the intermediate exciton states over which sums are taken, these intermediate exciton states just helping to visualize the precise exchange process at hand.

5.1 Generalized carrier exchanges

This led us to think that carrier exchanges involving $p = 2, 3, 4, \ldots$ excitons had to appear through generalized scatterings defined as

$$L_2\begin{bmatrix} m_2\ i_2 \\ m_1\ i_1 \end{bmatrix} = \int d\{\mathbf{r}\}\phi^*_{m_1}(\mathbf{r}_{e_1},\mathbf{r}_{h_1})\phi^*_{m_2}(\mathbf{r}_{e_2},\mathbf{r}_{h_2}) \times \phi_{i_1}(\mathbf{r}_{e_1},\mathbf{r}_{h_2})\phi_{i_2}(\mathbf{r}_{e_2},\mathbf{r}_{h_1}), \qquad (55)$$

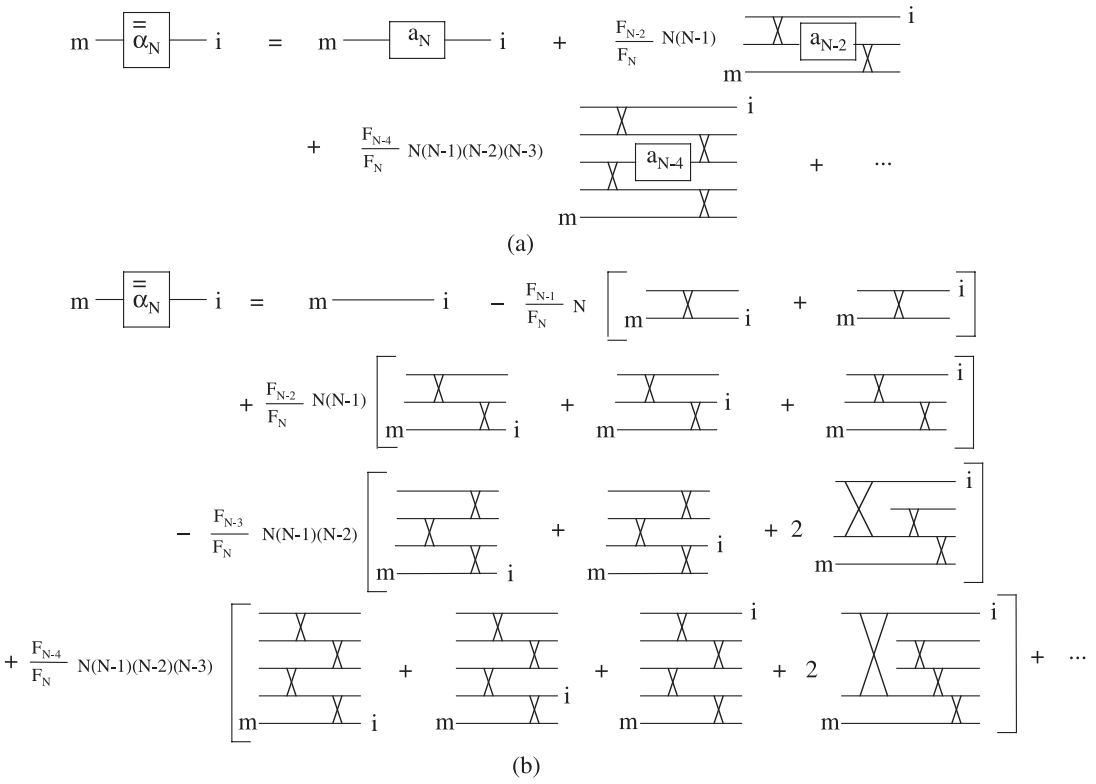

Fig. 12. (a): Diagrammatic expansion of the $\overline{\overline{\alpha}}_N(m,i)$ part of $A_N(m,i)$ which exists even if $\mathbf{Q}_m = \mathbf{Q}_i \neq \mathbf{Q}_0$, as it appears when we use the recursion relation between $A_N(m,i)$ and $A_{N-2}(n,j)$. These diagrams correspond to the iteration of equation (53). (b): Pauli diagrams for this $\overline{\overline{\alpha}}_N(m,i)$ as obtained by inserting the diagrams of Figure 3b for $a_N(m,i)$ into Figure 12a. The zeroth, first and second order Pauli diagrams of $\overline{\overline{\alpha}}_N(m,i)$ are identical to the ones of $\alpha_N(m,i)$ shown in Figure 5. However, at higher orders, these Pauli diagrams become more and more different. They however have to represent exactly the same quantity, since, as $\overline{\overline{\beta}}_N(m,i) = \beta_N(m,i)$, we must have $\overline{\overline{\alpha}}_N(m,i) = \alpha_N(m,i)$ for *any* N.

$$L_3 \begin{bmatrix} m_3\ i_3 \\ m_2\ i_2 \\ m_1\ i_1 \end{bmatrix} = \int d\{\mathbf{r}\} \phi^*_{m_1}(\mathbf{r}_{e_1}, \mathbf{r}_{h_1}) \phi^*_{m_2}(\mathbf{r}_{e_2}, \mathbf{r}_{h_2}) \times \phi^*_{m_3}(\mathbf{r}_{e_3}, \mathbf{r}_{h_3}) \phi_{i_1}(\mathbf{r}_{e_1}, \mathbf{r}_{h_2}) \phi_{i_2}(\mathbf{r}_{e_3}, \mathbf{r}_{h_1}) \phi_{i_3}(\mathbf{r}_{e_2}, \mathbf{r}_{h_3}), \quad (56)$$

$$L_4 \begin{bmatrix} m_4\ i_4 \\ m_3\ i_3 \\ m_2\ i_2 \\ m_1\ i_1 \end{bmatrix} = \int d\{\mathbf{r}\} \phi^*_{m_1}(\mathbf{r}_{e_1}, \mathbf{r}_{h_1}) \phi^*_{m_2}(\mathbf{r}_{e_2}, \mathbf{r}_{h_2}) \times \phi^*_{m_3}(\mathbf{r}_{e_3}, \mathbf{r}_{h_3}) \phi^*_{m_4}(\mathbf{r}_{e_4}, \mathbf{r}_{h_4}) \times \phi_{i_1}(\mathbf{r}_{e_1}, \mathbf{r}_{h_2}) \phi_{i_2}(\mathbf{r}_{e_3}, \mathbf{r}_{h_1}) \phi_{i_3}(\mathbf{r}_{e_2}, \mathbf{r}_{h_4}) \phi_{i_4}(\mathbf{r}_{e_4}, \mathbf{r}_{h_3}), \quad (57)$$

and so on... These definitions are in fact transparent if we look at the skeleton diagrams which represent them in Figure 13: The excitons of the lowest line (m_1, i_1) have the same electron but a different hole, and so on... Note that it is actually possible to represent these generalized carrier exchanges in various equivalent ways, as shown in Figure 14 in the case of three excitons. These equivalent representations simply say that the exciton i_1 has the same electron as the exciton m_1 and the same hole as the exciton m_2, so that i_1 and m_1 must be connected by an electron line while i_1 and m_2 must be connected by a hole line.

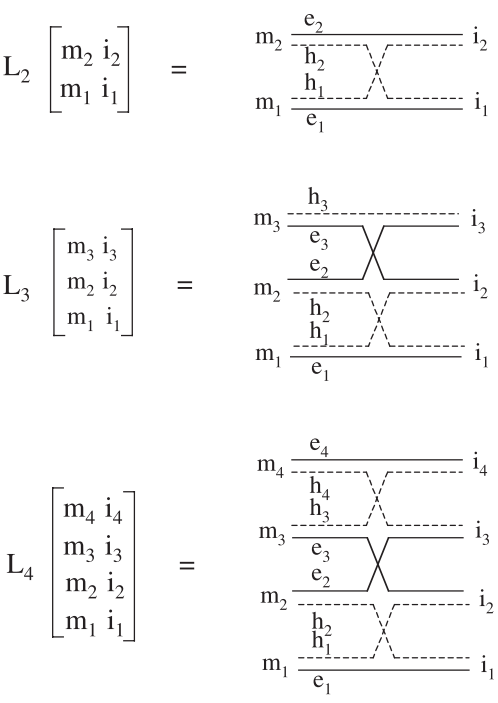

Fig. 13. Generalized carrier exchanges L_p between $p = 2, 3, 4$ excitons, as defined in equations (55−57).

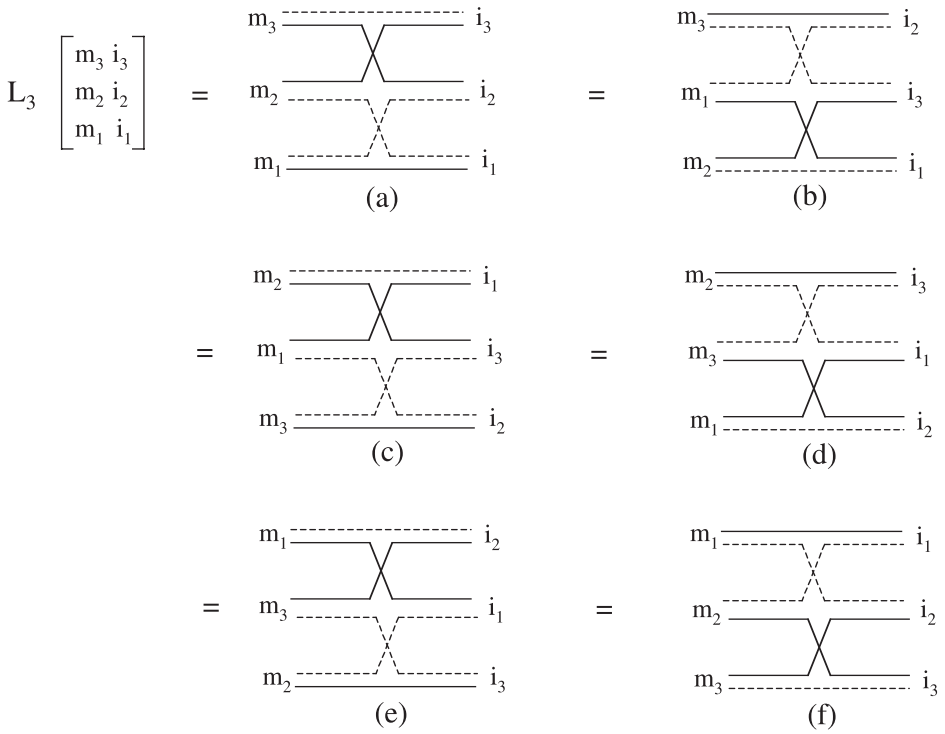

Fig. 14. Various possible representations of the *same* exchange process between three excitons, corresponding to the integral of equation (56). In all of them, the exciton m_1 is connected to the exciton i_1 by an electron line, these excitons (m_1, i_1) having the same electron, while it is connected to the exciton i_2 by a hole line, the excitons (m_1, i_2) having the same hole. And so on...

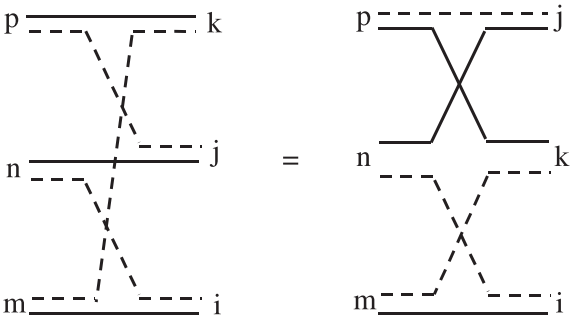

Fig. 15. A possible carrier exchange between the excitons (m, n, p) and (i, j, k), redrawn using the skeleton diagram between three excitons. The positions of (j, k) are just exchanged.

It is actually possible to represent all carrier exchanges between N excitons by such skeleton diagrams: The Pauli scattering between two excitons which appears in our many-body theory for composite excitons, simply reads $\lambda_{mnij} = \left[L_2 \begin{pmatrix} n & j \\ m & i \end{pmatrix} + L_2 \begin{bmatrix} m & j \\ n & i \end{bmatrix}\right)/2$ (see Fig. 1). In the same way, the carrier exchange between three excitons shown in Figure 15, is nothing but the skeleton diagram $L_3[(m,i);(n,k);(p,j)]$ in which the positions of j and k are just exchanged. A similar redrawing can actually be done for any other carrier exchange we could think of.

Let us now come back to the various Pauli diagrams we have found in calculating $A_N(m,i)$ and understand why they are indeed equivalent, in the light of these skeleton diagrams.

5.2 Pauli diagrams with one exciton only different from 0

Let us start with the simplest of these Pauli diagrams, namely the zigzag diagram $z^{(p)}(m,0)$ appearing in Figure 2, which has p excitons 0 and one exciton m on its left and $(p+1)$ excitons 0 on its right. After summation over the intermediate exciton indices, the final expression of this Pauli diagram must read as an integral of $\phi^*_m(\mathbf{r}_{e_1}, \mathbf{r}_{h_1})\phi^*_0(\mathbf{r}_{e_2}, \mathbf{r}_{h_2}) \ldots \phi^*_0(\mathbf{r}_{e_{p+1}}, \mathbf{r}_{h_{p+1}})$ multiplied by $(p+1)$ wave functions ϕ^*_0 with the $(\mathbf{r}_{e_i}, \mathbf{r}_{h_i})$'s mixed in such a way that the integral is not cut into two independent integrals (otherwise the Pauli diagram would not be topologically connected). This is exactly what $L_{p+1}[(m,0);(0,0);\cdots;(0,0)]$ does. The possible permutations of the various $(\mathbf{r}_e, \mathbf{r}_h)$'s in the definition of L_{p+1} show that the position of the m index in the diagrammatic representation of this carrier exchange is unimportant. As a consequence, the position of m in the Pauli diagrams having all the indices but one equal to 0, is unimportant. The relative position of the crosses in these diagrams is also unimportant. This is easy to show, just by "sliding" the carrier exchanges, as explained in Figure 16 in the case of three excitons. In this figure, we use the fact that the two carrier exchanges of the Pauli scattering λ_{mnij} reduce to one diagram when two indices on one side are

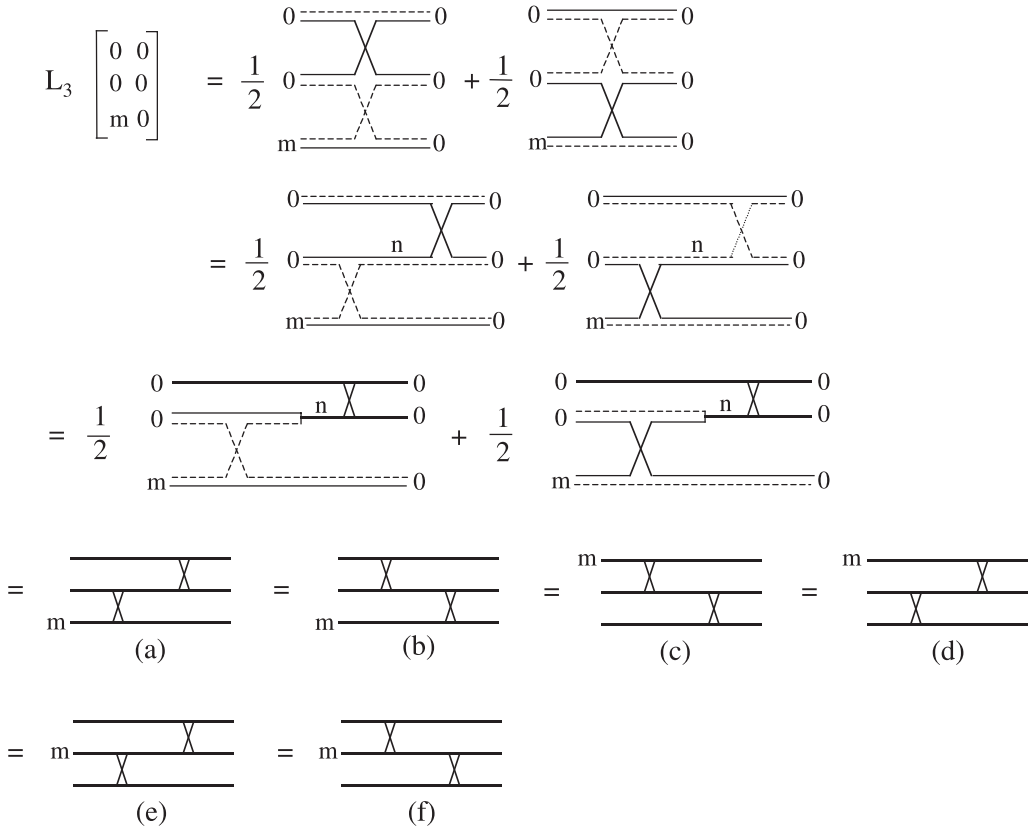

Fig. 16. The skeleton diagram for three excitons, with all excitons but one in the same state 0, corresponds to one of the two equivalent diagrams of the first line of this figure, due to Figure 14; so that it is also half their sum. In the second line, we have just "slided" the carrier exchanges. In the third line, we use the fact that, when the two indices on one side of a Pauli scattering are equal, this Pauli scattering, here λ_{n000}, corresponds either to an electron exchange or to a hole exchange. The Pauli diagram (a) of this figure then results from using Figure 1a for λ_{m00n}. If we slide the carrier exchanges the other way, we end with the Pauli diagram (b). Diagram (c) is obtained from (a) by a symmetry up-down which follows from $\lambda_{mnij} = \lambda_{nmji}$; and similarly for diagram (d) starting from (b). In the same way, the diagram (e) follows from (a) due to $\lambda_{m00n} = \lambda_{0m0n}$, while the diagram (f) follows from (c) for the same reason. This shows that all Pauli diagrams with only one index different from 0, correspond to the same skeleton diagram, whatever the positions of m and the Pauli scatterings are, a remarkable result, not topologically obvious at first.

equal (see Figs. 1d, e). This possibility to "slide" the carrier exchange, mathematically comes from the fact that $\sum_q \phi_q^*(\mathbf{r}_e, \mathbf{r}_h)\phi_q(\mathbf{r}_{e'}, \mathbf{r}_{h'})$ is just $\delta(\mathbf{r}_e - \mathbf{r}_{e'})\delta(\mathbf{r}_h - \mathbf{r}_{h'})$.

5.3 Pauli diagrams with one exciton different from 0 on each side

There are essentially two kinds of such diagrams: Either the two excitons (m, i) different from 0 have one common carrier, or they have none. Let us start with the first case.

5.3.1 m and i have one common carrier

Two topologically different skeleton diagrams exist in this case, depending if the common carrier is an electron or a hole. They are shown in Figures 17a, b. By "sliding" the carrier exchanges as done in Figure 17c, we can identify the set of Pauli diagrams which correspond to the sum of these two skeleton diagrams (see Fig. 17d). This in particular shows the identity of the Pauli diagrams which enter the two diagrammatic representations of $a_N(m, i)$ shown in Figures 3b, c.

5.3.2 m and i have no common carrier

The number of topologically different skeleton diagrams depends on the number of excitons 0 involved. In the case of two excitons 0, there is only one such skeleton diagram (see Fig. 18). By "sliding" the carrier exchanges, we get the two equivalent Pauli diagrams of this figure. For three excitons 0, we have the two different skeleton diagrams shown in Figures 19a, b. They are related by exchanging the electrons and holes. By sliding the carrier exchanges, we get the two diagrams of Figure 19c; so that, if we combine these two skeleton diagrams, we end with the two Pauli diagrams of Figure 19d, which are thus equivalent, in spite of the position of the crosses.

And so on...

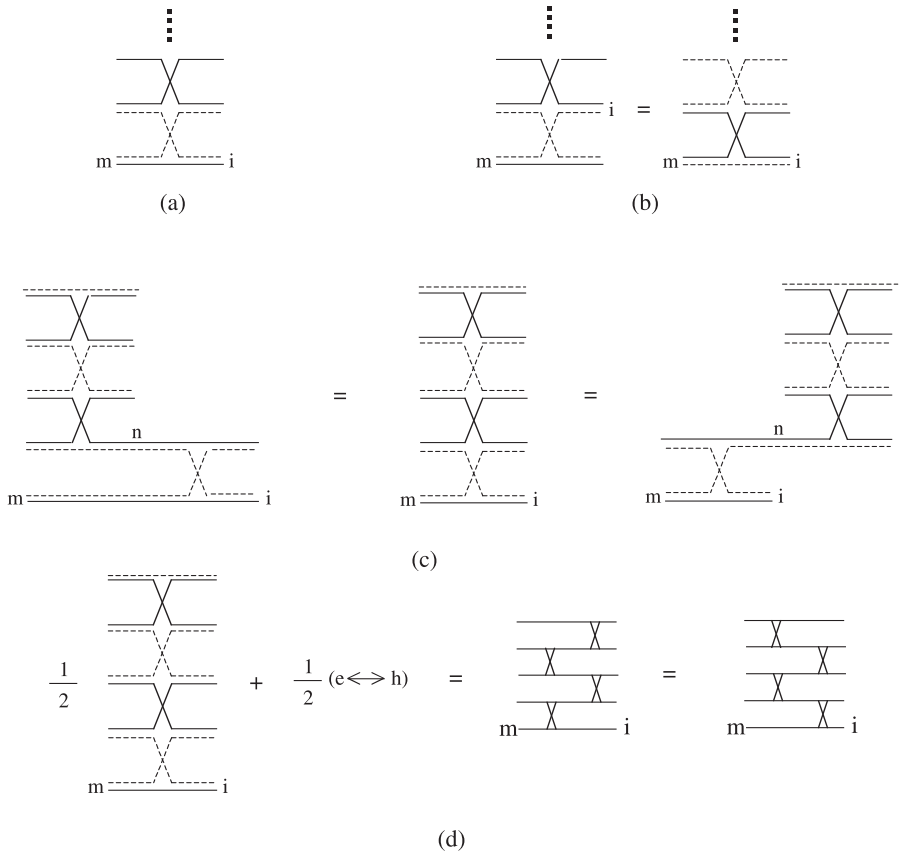

Fig. 17. (a, b): Skeleton diagrams in which the excitons m and i have the same electron (a) or the same hole (b). (c): When all the other indices are 0, we can slide the carrier exchange one way or the other to identify a skeleton diagram for which all the indices except one are 0: The upper part thus corresponds to a Pauli diagram with the n index and the crosses for Pauli scatterings put at any place. (d): If we now add the electron exchange to the hole exchange, in order to get the two parts of the Pauli scattering, λ_{m0in} or λ_{mni0}, we end with the two Pauli diagrams of Figures 3b, c for $a_N(m,i)$: The two zigzag diagrams are indeed equal.

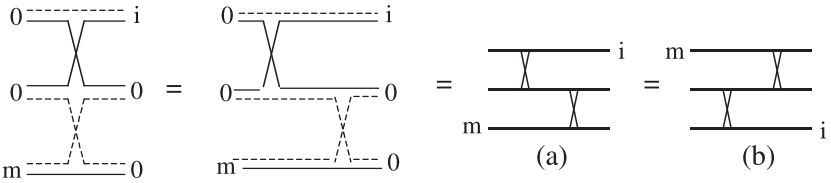

Fig. 18. In the case of three excitons, there is only one skeleton diagram in which m and i have no common carrier. If the other excitons are excitons 0, we can slide the electron exchange to the left to make appearing two Pauli scatterings having equal indices on one side. Using Figures 1d and 1e, we then find that this skeleton diagram corresponds to the Pauli diagram (a). A symmetry up-down leads to diagram (b).

5.4 Equivalent representations of the diagrams appearing in $A_N(m,i)$

By expressing the various Pauli diagrams entering the expansion of $A_N(m,i)$, in terms of skeleton diagrams, it is now possible to directly prove their equivalence.

Figure 20 shows the set of transformations which allows to go from the last third order diagrams of $\overline{\overline{\alpha}}_N(m,i)$, shown in Figure 12b, to the two zigzag Pauli diagrams of $\alpha_N(m,i)$, with i at the two upper positions.

The transformation of the last fourth order diagram for $\overline{\overline{\alpha}}_N(m,i)$ into the two missing zigzag diagrams of $\alpha_N(m,i)$ is somewhat more subtle. For the interested reader, it is explained in details in the caption of Figure 21.

6 Conclusion

In this paper, we have calculated the scalar product of $(N+1)$-exciton states with N of them in the same state 0. This scalar product is far from trivial due to

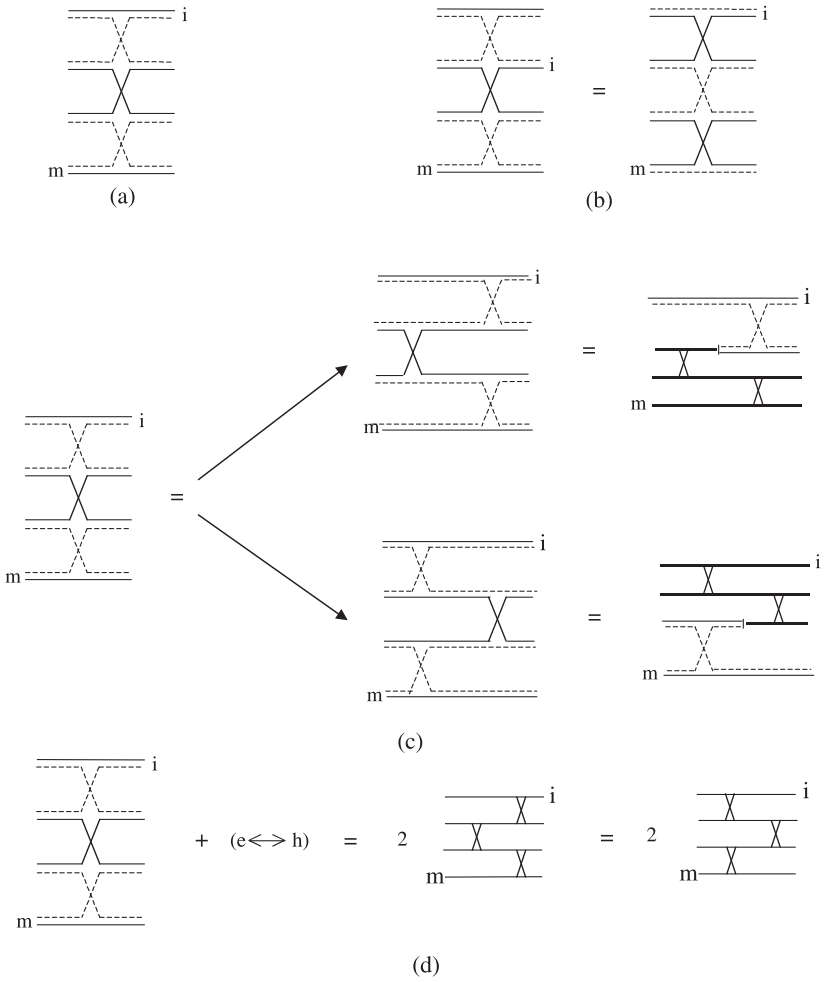

Fig. 19. (a, b): In the case of four excitons, there are two different skeleton diagrams in which the excitons m and i have no common carrier. (c): Starting from the skeleton diagram (a), we can slide the carrier exchanges one way or the other, to make appearing Pauli scatterings with two excitons 0 on one side. By combining the two skeleton diagrams (a) and (b), we generate the two parts of λ_{n00i} (or λ_{m00n}): This produces the two Pauli diagrams (d), which just differ by the position of the zigzags, right, left, right or left, right, left.

many-body effects induced by *"Pauli scatterings"* which originate from the composite nature of the excitons. As a result, these scalar products appear as expansions in $\eta = N\mathcal{V}_X/\mathcal{V}$, where $\mathcal{V}_X$ and $\mathcal{V}$ are the exciton and sample volumes, with possibly some additional factors N.

In order to understand the physical origin of these additional N's — which will ultimately differentiate superextensive from regular terms — we have introduced the concept of *"exciton dressed by a sea of N excitons 0"*,

$$|\psi_i^{(N)}\rangle = \frac{B_0^N B_0^{\dagger N}}{\langle v|B_0^N B_0^{\dagger N}|v\rangle}\, B_i^\dagger|v\rangle.$$

If the excitons are replaced by true bosons, the excitons $i \neq 0$ are unaffected by the sea, while the exciton 0 is enhanced by a factor N. If we drop all Pauli interactions between the exciton i and the sea, the operator in front of $B_i^\dagger$ reduces to an identity, so that all excitons i are unchanged. If we now take into account Pauli interactions between composite excitons properly, we find that all dressed excitons i gain a contribution on other excitons $m \neq i$, due to possible carrier exchanges between the exciton i and the sea. Moreover, we find that a N bosonic enhancement exists not only for the exciton $i = 0$ — which is, after all, rather satisfactory since excitons are not so far from bosons — but also for any exciton i which can be transformed into a sea exciton by carrier exchanges, i.e., any exciton i having a center of mass momentum equal to the one of a sea exciton.

In order to understand the carrier exchanges between N excitons — which make the scalar products of N-exciton states so tricky —, we have first used *"Pauli diagrams"*, i.e., diagrams written in terms of *Pauli scatterings between two excitons*. With them, we have succeeded in generating a diagrammatic representation of the scalar products of $(N+1)$-exciton states with N of them in the same state 0, at any order in Pauli interaction.

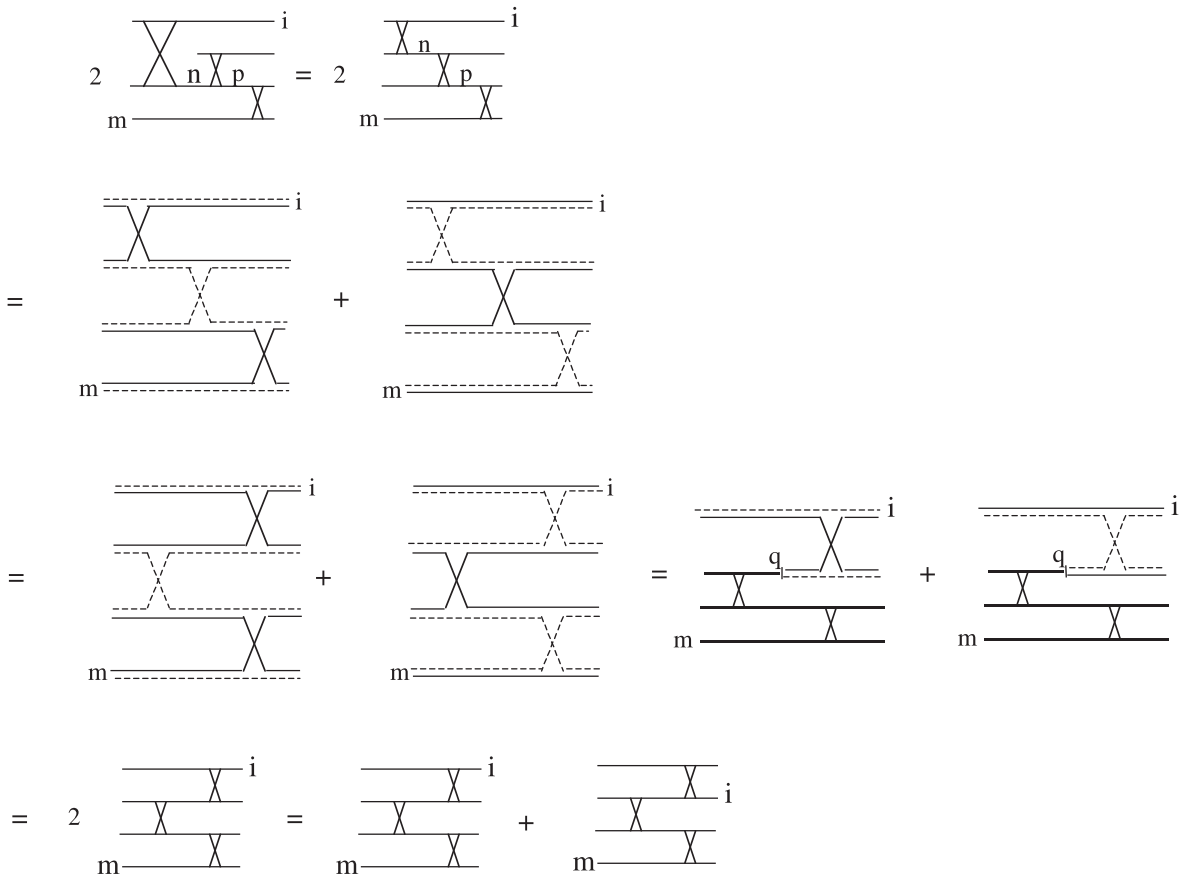

Fig. 20. In this figure, we show how to transform the last third order Pauli diagram of $\overline{\overline{\alpha}}_N(m,i)$ appearing in Figure 12b, into the two zigzag diagrams of Figure 5c for $\alpha_N(m,i)$, which are reproduced at the bottom of this figure. We first use the fact that $\lambda_{n0p0} = \lambda_{0np0}$ to get an equivalent representation of this diagram. We then note that the upper and lower crosses have two identical excitons on one side. By using Figures 1d, e for the two upper crosses, and Figures 1a, b for the middle cross, we get the two diagrams of the second line of this figure. The diagrams of the next line just follow by sliding the carrier exchanges. In them, we now identify Pauli scatterings which have identical excitons on one side. These two diagrams can be used to generate the two parts of the Pauli scattering λ_{q00i}. The sum of the last two zigzag diagrams simply results from $\lambda_{q00i} = \lambda_{q0i0}$.

This diagrammatic representation is actually not unique, which makes it quite unsatisfactory. Although the one we first give is simple to memorize, due to its nice topology, more complicated ones, obtained from other procedures to calculate the same scalar product, are equally good in the sense that they lead to the same correct result.

In order to understand the equivalence between these various Pauli diagrams, we have been led to introduce *"skeleton diagrams"* which correspond to *carrier exchanges between more than two excitons*. Their appearance in the scalar products of N-exciton states is actually quite reasonable because, even if we can calculate these scalar products in terms of Pauli scatterings between *two* excitons only, Pauli exclusion is originally N-body: When a new exciton is added, its carriers must be in states different from the ones of *all* previous excitons. The Pauli scatterings between two excitons generated by our many-body theory for interacting composite bosons, are, for sure, mathematically convenient to calculate many-body effects between excitons at any order in carrier exchanges. It is however reasonable to find that a set of such Pauli scatterings, which correspond to carrier exchanges between more than two excitons, finally read in terms of these skeleton diagrams, designed to describe multiple exchanges.

The present work is restricted to scalar products of N-exciton states in which all but one are in the same state 0. In physical effects involving N excitons, more complicated scalar products of course enter. Their calculation will be presented in a forthcoming publication. The detailed study presented here, is however quite useful: Beside the skeleton diagrams this study led us to identify, it allowed us to point out one very important characteristic of these scalar products, linked to the topology of their diagrammatic representation — also present in more complicated situations: For example, in the case of two excitons (i,j) dressed by a sea of N excitons 0 in the same way as equation (12), a bosonic enhancement exists not only for $\mathbf{Q}_i = \mathbf{Q}_j = \mathbf{Q}_0$, but also for $\mathbf{Q}_i + \mathbf{Q}_j = 2\mathbf{Q}_0$, because

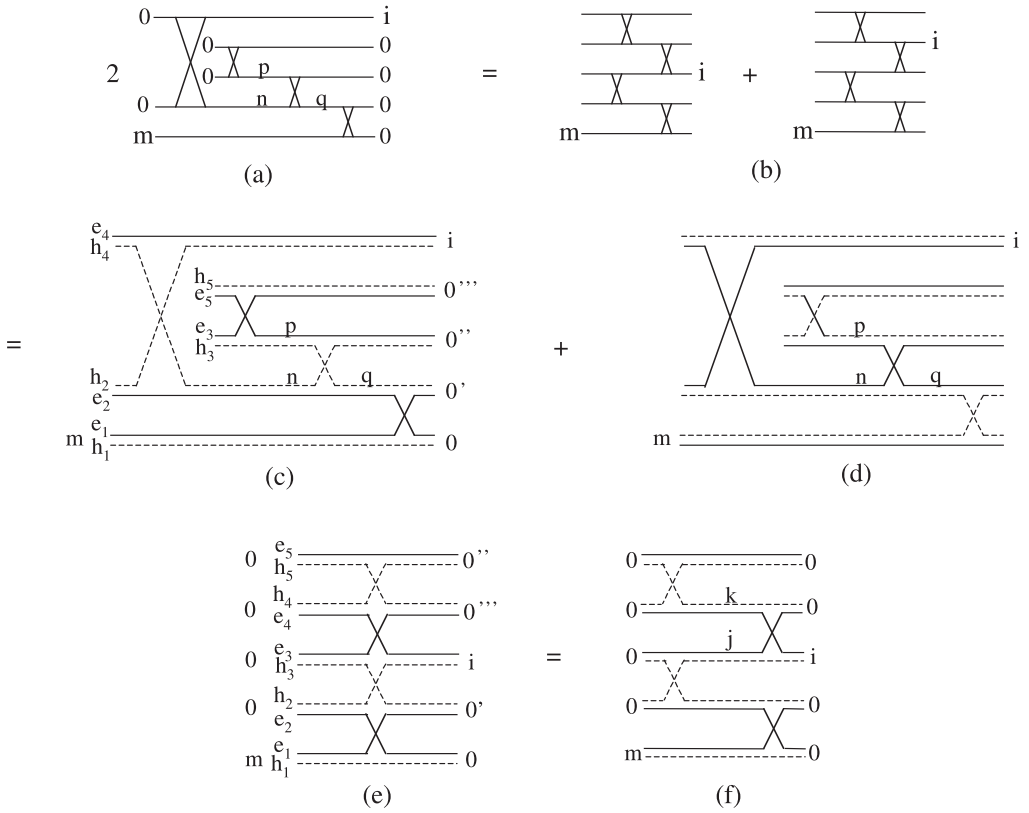

Fig. 21. The transformation of the quite ugly fourth order Pauli diagram appearing in $\overline{\overline{\alpha}}_N(m,i)$ and reproduced in (a), into the two zigzag diagrams of $\alpha_N(m,i)$ reproduced in (b), is actually quite subtle. In diagram (a), all the Pauli scatterings except λ_{npq0} have two indices 0 on one side. This allows to transform twice the diagram (a) into the sum of diagrams (c) and (d), using Figures 1a, b and Figures 1d, e. Diagram (c) is nothing but diagram (e) as easy to see by following the various electron and hole lines labelled differently, in order to easily check that excitons with identical electrons (or holes) are indeed connected. We then slide the carrier exchange to produce diagram (f). This diagram has Pauli scatterings with two excitons 0 on one side, except the one between (j,k) and $(i,0)$. By doing the same for diagram (d), we generate the two parts of the Pauli scattering λ_{jk0i}. The two diagrams shown in (b) then simply follow from $\lambda_{jk0i} = \lambda_{jki0}$.

this last condition is enough for the two excitons (i,j) to possibly transform themselves into two excitons 0 by carrier exchanges; the corresponding process, represented by topologically disconnected diagrams, appears with an extra factor N, which is the signature of this topology.

References

1. M. Combescot, C. Tanguy, Europhys. Lett. **55**, 390 (2001)
2. M. Combescot, O. Betbeder-Matibet, Europhys. Lett. **58**, 87 (2002)
3. O. Betbeder-Matibet, M. Combescot, Eur. Phys. J. B **27**, 505 (2002)
4. M. Combescot, O. Betbeder-Matibet, Europhys. Lett. **59**, 579 (2002)
5. M. Combescot, X. Leyronas, C. Tanguy, Eur. Phys. J. B **31**, 17 (2003)
6. O. Betbeder-Matibet, M. Combescot, Eur. Phys. J. B **31**, 517 (2003)
7. M. Combescot, O. Betbeder-Matibet, K. Cho, H. Ajiki, `cond-mat/0311387`
8. A.A. Abrikosov, L.P. Gorkov, I.E. Dzyaloshinski, *Methods of quantum field theory in statistical physics* (Prentice-hall, inc. Englewood cliffs N.J., 1964)
9. F. Pistolesi, G.C. Strinati, Phys. Rev. B **53**, 15168 (1996)
10. P. Pieri, G.C. Strinati, Phys. Rev. B **61**, 15370 (2000)
11. C. Cohen-Tannoudji, B. Diu, F. Laloë, *Mécanique Quantique* (Hermann, Paris, 1973)